Journal of Medicinal Chemistry

Article

Suppression of Drug-Resistant Non-Small-Cell Lung Cancer with Inhibitors Targeting Minichromosomal Maintenance Protein

Chia-Yi Lin, Hsin-Yi Wu, Yuan-Ling Hsu, Ting-Jen Rachel Cheng, Jyung-Hurng Liu, Rou-Jie Huang, Tzu Hung Hsiao, Chia-Jen Wang, Pei-Fang Hung, Albert Lan, Szu-Hua Pan, rj Chein, Chi-Huey Wong, and Pan-Chyr Yang

J. Med. Chem., **Just Accepted Manuscript** • DOI: 10.1021/acs.jmedchem.9b01783 • Publication Date (Web): 03 Mar 2020

Just Accepted

is published by the American Chemical Society. 1155 Sixteenth Street N.W., Washington, DC 20036

Suppression of Drug-Resistant Non-Small-Cell Lung Cancer with Inhibitors Targeting Minichromosomal Maintenance Protein

*Chia-Yi Lin,[1, 2] Hsin-Yi Wu,[3] Yuan-Ling Hsu,[4] Ting-Jen Rachel Cheng,[5] Jyung-Hurng Liu, [6, 7, 8] Rou-Jie Huang,[9] Tzu Hung Hsiao,[10] Chia-Jen Wang,[11] Pei-Fang Hung,[2] Albert Lan,[4] Szu-Hua Pan,[1, 4, 12,] * Rong-Jie Chein,[3,] * Chi-Huey Wong,[5] and Pan-Chyr Yang[1, 2, 13]*

1. Genome and Systems Biology Degree Program, National Taiwan University and Academia Sinica, Taipei 100, Taiwan
2. Institute of Biomedical Sciences, Academia Sinica, Taipei 115, Taiwan
3. Institute of Chemistry, Academia Sinica, Taipei 115, Taiwan
4. Graduate Institute of Medical Genomics and Proteomics, College of Medicine, National Taiwan University, Taipei 100, Taiwan
5. The Genomics Research Center, Academia Sinica, Taipei 115, Taiwan
6. Institute of Genomics and Bioinformatics, College of Life Sciences, National Chung Hsing University, Taichung 402, Taiwan
7. Agricultural Biotechnology Center, NCHU, Taichung 402, Taiwan
8. Rong Hsing Research Center for Translational Medicine, NCHU, Taichung 402, Taiwan
9. Department of Chemistry, National Central University, Jhong-Li 320, Taiwan
10. Department of Medical Research, Taichung Veterans General Hospital, Taichung 407, Taiwan
11. Institute of Stem Cell and Translational Cancer Research, Chang Gung Memorial Hospital, Taoyuan 333, Taiwan.
12. Doctoral Degree Program of Translational Medicine, National Taiwan University, Taipei 100, Taiwan
13. Department of Internal Medicine, College of Medicine, National Taiwan University, Taipei 100, Taiwan

∗ Corresponding authors

KEYWORDS

Minichromosomal maintenance protein (MCM), DNA replication, cell cycle, and lung cancer

ABSTRACT

Drug resistance has been a major threat in cancer therapies that necessitates the development of new strategies to overcome this problem. We report here a cell-based high-throughput screen of a library containing 2-million molecules for the compounds that inhibit the proliferation of non-small-cell lung cancer (NSCLC). Through the process of phenotypic screening, target deconvolution and structure-activity relationship (SAR) analysis, a compound of furanonaphthoquinone-based small molecule, AS4583, was identified which exhibited potent activity in tyrosine kinase inhibitor (TKI)–sensitive and TKI–resistant NSCLC cells (IC_{50} 77 nM) and in xenograft mice. The mechanistic studies revealed that AS4583 inhibited cell-cycle progression and reduced DNA replication by disrupting the formation of the minichromosomal maintenance protein (MCM) complex. Subsequent SAR study of AS4583 gave compound RJ-LC-07-48 which exhibited greater potency in drug-resistant NSCLC cells (IC_{50} 17nM) and in mice with H1975 xenograft tumor.

INTRODUCTION

Lung cancer remains the leading cause of cancer-related death worldwide, and approximately 1.8 million new lung-cancer cases are diagnosed every year[1], the majority being non-small-cell lung cancer (NSCLC). Despite advances in cancer treatment have been made over the past 20 years, less than 30% of lung-cancer patients respond to chemotherapy, and prognoses generally remain poor[2, 3]. Although the development of specific tyrosine kinase inhibitors (TKIs) targeting the epidermal growth factor receptor (EGFR) has improved patient outcomes, drug resistance has become a major

concern. Therefore, it is essential to develop new anticancer agents with novel mode of action to overcome the problem of drug resistance, especially of EGFR-TKI resistance.

Over the last years, target-based screens and cell-based screens have been the two predominant strategies for drug discovery. With the growing knowledge of cancer biology, many pharmaceutical companies have used target-based screens to develop therapeutic agents that specifically inhibit the key factors associated with cancer progression[4], e.g., the FDA-approved drugs gefitinib[5], erlotinib[6] (targeting EGFR), crizotinib[7] (targeting MET and ALK), imatinib[8] (targeting ABL), temsirolimus[9] (targeting mTOR) and dabrafenib[10] (targeting BRAF). However, the problem of drug resistance and the number of known targets that drive cancer progression remains limited, presenting a substantial challenge for target-based drug development[11]. In order to identify new targets for the development of anticancer agents, the strategy of cell-based phenotypic screens has been used and several anticancer agents have been developed and approved by the FDA, e.g., vorinostat[12], romidepsin[13], azacitidine[14], lenalidomide and pomalidomide[15].

Recently, the integration of high-throughput or high-content screening of large libraries combined with computational data mining has been used to facilitate the drug discovery process, including target identification and validation as well as the study of structure-activity relationship (SAR) and mechanisms of action[16]. Herein, we present a successful hit-to-lead discovery of a novel anticancer compound with high potency against both TKI-sensitive and TKI-resistant NSCLC using cell-based, high-throughput screening combined with SAR study and *in silico* modeling and simulation. A high-throughput screen of lung-cancer cells with different EGFR mutation status[17] was

performed to identify compound AS4583, a furanonaphthoquinone-based small molecule, that interferes with S-phase progression. *In vitro* analyses indicated that AS4583 interferes with cell-cycle progression and DNA replication by disrupting the formation of the minichromosomal maintenance protein (MCM) complex by promoting the proteasome degradation, especially of MCM2. Further SAR study of AS4583 led to the identification of RJ-LC-07-48 with anticancer efficacy around 10-fold higher than AS4583 against TKI-resistant NSCLC.

RESULTS

Identification of AS4583 as an inhibitor of NSCLC cell proliferation

A high-throughput screening of 2 million compounds (each 10 μM) was initially carried out to evaluate their ability to inhibit the proliferation of human H1975 NSCLC cells, which are resistant to EGFR-TKIs and harbor an EGFR-TKI-sensitive mutation (L858R) and an acquired resistance mutation (T790M)[18]. Approximately 6,800 hit compounds exhibited $\geq$ 80% inhibition at 10 μM were identified, which were further screened against other lung-cancer cells, including clinical isolates (CL1-0 and CL1-5) as well as an ATCC cell line PC9 and its EGFR-TKI-derivative–resistant clone PC9/IR. We then focused on compounds with potent activity against both TKI-sensitive and TKI-resistant cells, such as PC9 and PC9/IR, respectively, to identify compounds with new modes of action. After excluding established anticancer drugs, such as topotecan and doxorubicin analogs, a total of 193 hits with $\geq$80% inhibition at 10 μM were identified and further assessed with respect to their ability to inhibit the proliferation of both normal and cancer cells, especially inhibition of cell-cycle progression. Among them, a furanonaphthoquinone-based small molecule, AS4583 (Figure 1A), was found to inhibit the proliferation of both TKI-sensitive and TKI-resistant lung-cancer cells with IC_{50} values of <100 nM and more than 10-fold higher potency for cancer cells than human normal bronchial epithelial cells (NBE, Figure 1B and Table S1 and S2).

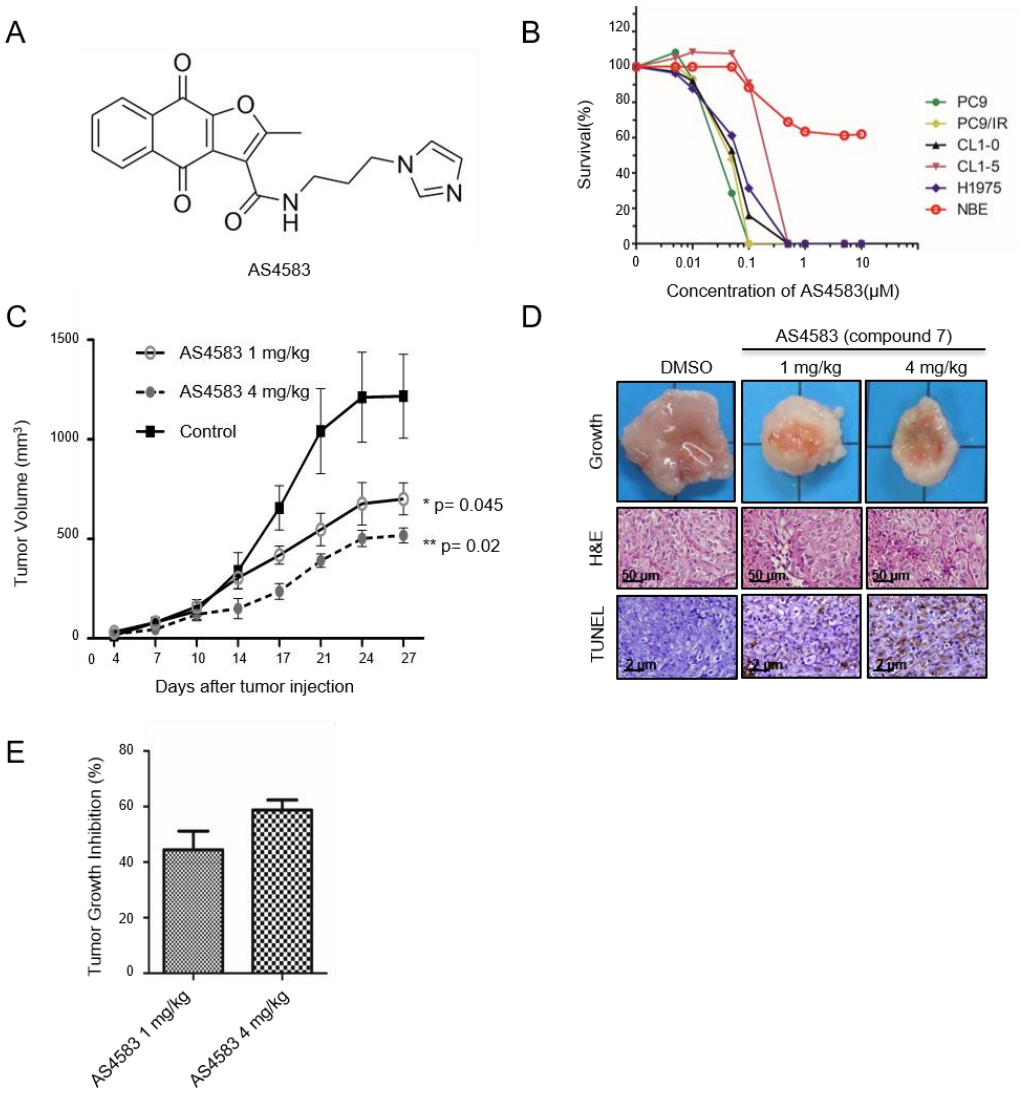

Figure 1. AS4583 selected from high-throughput screening affects cell proliferation and inhibits tumor growth *in vivo*. (A) Structure of AS4583. (B) Cytotoxicity assay for AS4583 with various normal and tumor cell lines. Cells were treated with 0–10 μM AS4583 for 72 h, and survival was assessed with the sulforhodamine B assay. (C) Tumor sizes and (D) TUNEL assay results from tumor xenograft models (n=6 per group). H1975 cells (3×10^6) were subcutaneously injected into male nu/nu mice. Tumor size was measured every 3 to 4 days. At day 27, the mice were sacrificed to examine tumor size as well as to confirm histology (original magnification 400×) and apoptosis status by hematoxylin and eosin (H&E) and TUNEL staining. (E) Bar graph comparing percent tumor growth inhibition (%TGI) on the day of the final measurement for the control group was compared across all treatments *in vivo* study

AS4583 inhibits tumor growth i*n vivo*

To evaluate the antitumor efficacy of AS4583 *in vivo*, athymic nude mice bearing established subcutaneous H1975 tumors were five days a week treated with 1 mg/kg or 4 mg/kg AS4583 (compared with DMSO control) for 4 weeks (n=6 per group). The result showed that treatment with AS4583 significantly reduced H1975 xenograft tumor growth on post-treatment day 27 (average tumor size, 1,217 ± 516.6 mm^3 for DMSO, 701.2 ± 196.5 mm^3 for 1 mg/kg, and 518.0 ± 93.0 mm^3 for 4 mg/kg, both $p<0.05$) and induced apoptosis in the tumor tissues (Figure 1C and 1D). Both AS4583 treatment induced tumor growth delay for a longer period of time when compared with DMSO controls. Compared to DMSO-treated animals, AS4583 1 mg/kg and 4 mg/kg showed significant percent tumor growth inhibition (% TGI) of 44 and 59, respectively (Figure 1E). To evaluate the potential cytotoxicity of AS4583, especially in liver and kidney, the body weight of each mouse was measured and the serum was subjected to biochemical analysis including aspartate transaminase, alanine transaminase, blood urea nitrogen, and creatinine (Supplementary Figure 1). No significant difference was observed. These results indicated that AS4583 could inhibit tumor growth without side effects.

AS4583 inhibits formation of the DNA replication fork and prolongs S phase in NSCLC cells

To examine the hypothesis that treatment of cells with AS4583 might disrupt cell cycle, we first performed a flow cytometry analysis to examine the effect of this compound on cell-cycle progression. H1975 cells treated with 140 nM AS4583 for 72 h were significantly arrested in the S phase (18% of the treated vs. 2% of the control group) and the G2/M phase (38% of the treated vs. 17% of the control group) (Table S3). Next, we investigated whether AS4583 inhibits cell proliferation by interfering with DNA replication. The incorporation of bromodeoxyuridine (BrdU) into replicated DNA was monitored in H1975 cells treated with DMSO (control) or AS4583 for 12, 24, or 48 h. The percentage of BrdU-positive cells was lower in the treated group (at 24 h: 27.7 ± 3.9% vs. 44.5 ± 2.0% for the control, p=0.086; at 48 h: 16.0 ± 2.5% vs. 34.0 ± 5.6% for the control, p= 0.0411; Figure 2A and 2B).

To further assess whether treatment with AS4583 interferes with DNA replication, we examined the formation of replication forks by immunofluorescence staining of the replication marker, MCM2, in both DMSO- and AS4583-treated H1975 cells released from G1 phase. Indeed, fewer replication forks were found in the AS4583-treated group (48.8 ± 18.7) compared with the control (176.8 ± 8.7, p= 0.0007, Figure 2C). Whether this decrease in the formation of replication forks could alter the distribution of cell-cycle phases was then evaluated. H1975 cells were synchronized in G1/S phase using a double thymidine block followed by release with DMSO and AS4583-containing medium up to 26 h. We observed that a higher percentage of AS4583-treated cells (p= 0.0373) remained in the G1/S phase after 20 h (Figure 2D), demonstrating that AS4583 increased the G1/S phase population, i.e., causing G1/S arrest. These results revealed that AS4583 significantly inhibits replication-fork progression and hence prevents cell-cycle progression.

When further dissecting the potential apoptotic pathways that are activated by AS4583, the expression levels of several specific apoptotic markers were detected by immunoblotting. As expected, the cleaved form of three important regulatory proteins in the apoptotic pathway, caspase-3 and PARP-1, appeared after AS4583 treatment. The appearance of cleaved caspase-8 implied that an intrinsic apoptotic pathway was being activated by AS4583 treatment (Figure 2E).

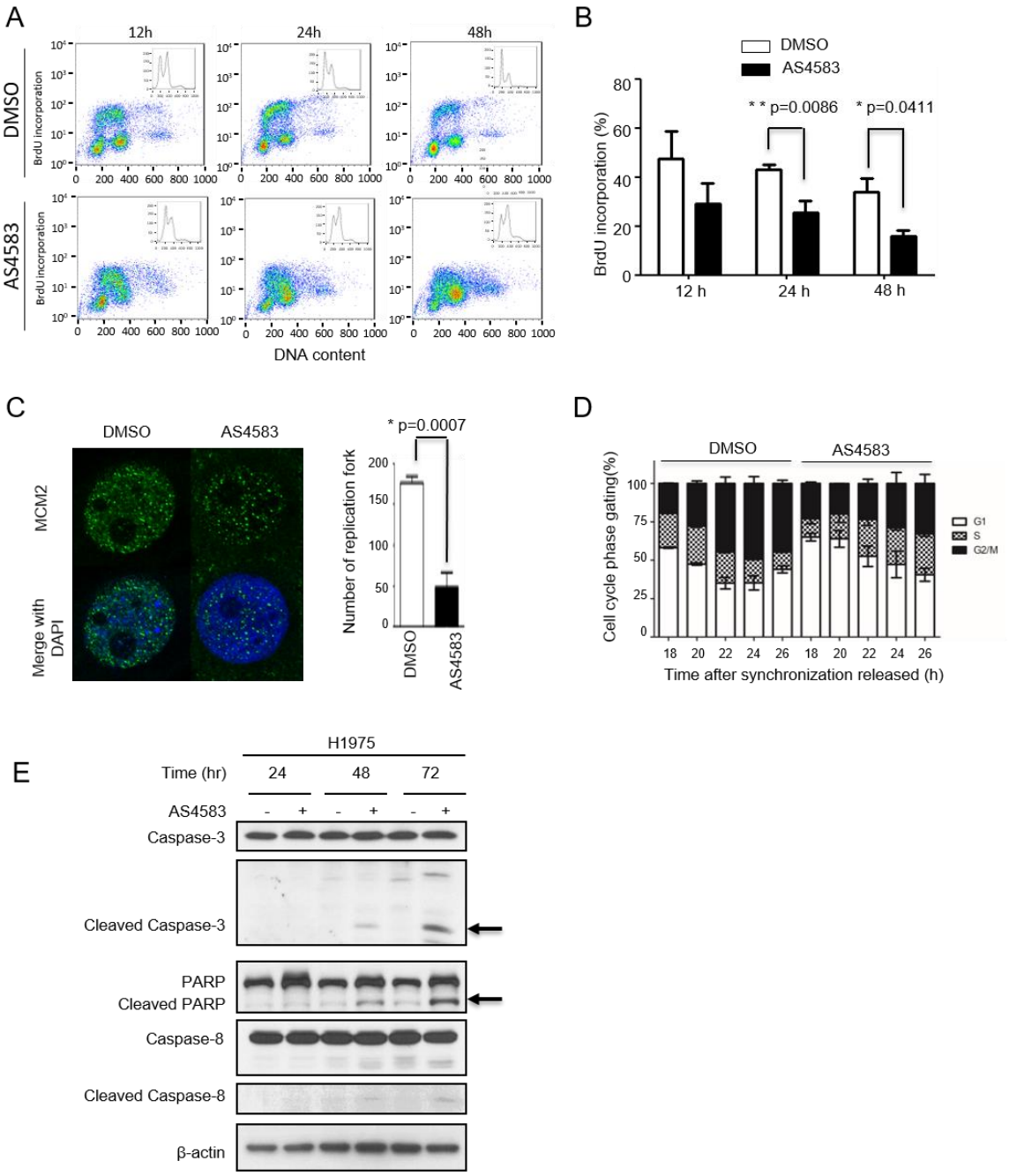

Figure 2. Treatment of cells with AS4583 interrupts DNA replication, causes cell cycle arrest and induces apoptosis. (A-B) AS4583 inhibits DNA replication in H1975 cells. H1975 cells were pulsed with BrdU and analyzed by flow cytometry. A: representative DNA histograms from DMSO- and AS4583-treated H1975 cells over time (three independent experiments). B: average percentage of cells in which BrdU was incorporated. (C) AS4583 decreases the number of DNA replication forks. The replication forks were analyzed by immunofluorescence staining for MCM2 (green) and DAPI (blue, for nuclei). Data were quantified by counting clear, green spots using Image J software (n=5 cells per group; original magnification, 1000×). (D) G1/S phase is prolonged in AS4583-treated H1975 cells. A double thymidine block was performed, and the data were collected at the indicated time points. (E) AS4583 induced intrinsic apoptosis pathway. H1975 cells were treated with AS4583 for 24, 48 or 72 h. The apoptotic marker protein expressions were detected by immunoblotting.

The decrease in MCM2 level could lead to cell death through silencing the expression of MCM2 via lentivirus-based short hairpin RNAs

As a significant reduction of MCM2 in AS4583 treated cells was observed in the DNA replication fork study, we were curious about whether the decrease of MCM2 could directly interfere in the cell survival. To test this hypothesis, we silenced the expression of MCM2 via lentivirus-based short hairpin RNAs, and then, confirmed whether the breakdown of MCM2 accounts for AS4583-induced cell death. The results showed that MCM2 knockdown resulted in a 33% inhibition of cell proliferation ($p< 0.0001$, Figure 3A), and the efficiency of knockdown depended on the amount of short hairpin RNA ($p< 0.0001$, Figure 3B). These data are consistent with the observations reported by Liang and his colleagues[19]. Moreover, we also found that AS4583-induced cell death correlated positively with the expression of MCM2 in different lung-cancer cell lines and skin fibroblast cell line (Figure 3C, 3D and Table S4). These data implied that MCM complex might be involved in AS4583 –induced lung cancer cell death.

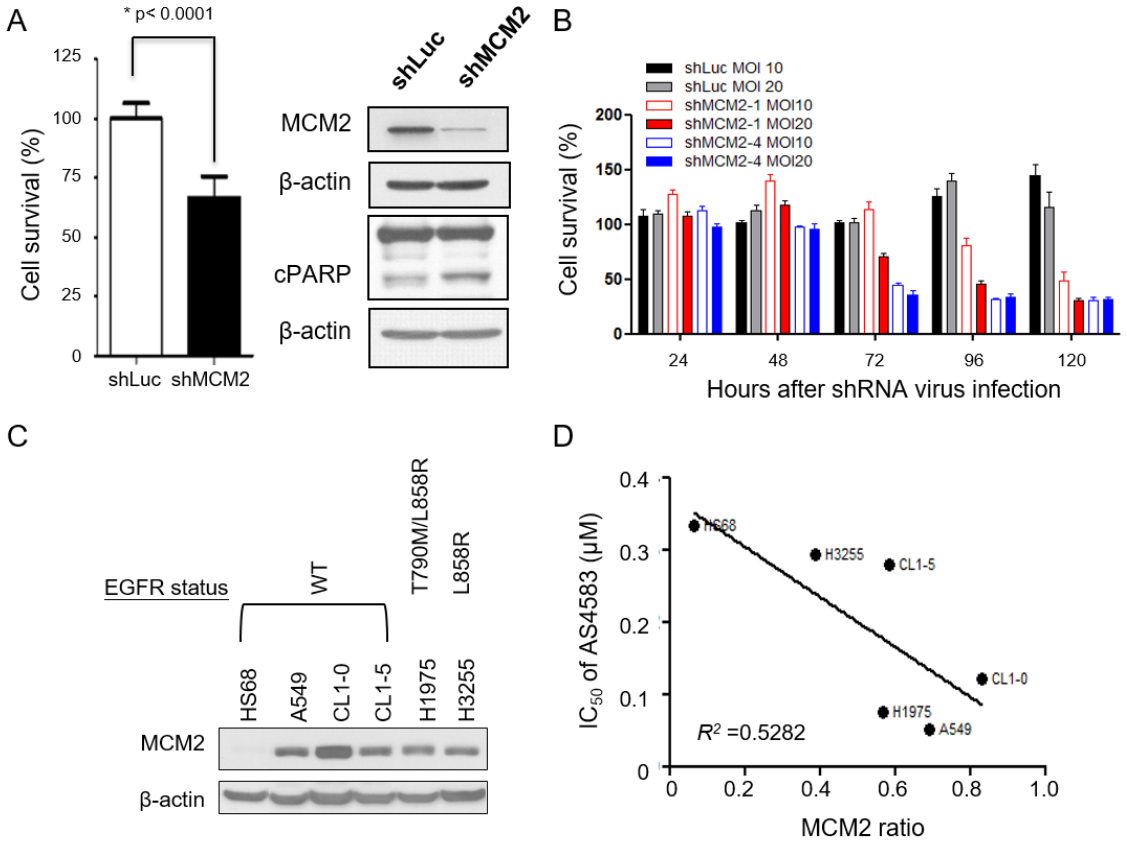

Figure 3. The correlation between MCM2 level and cell death via lentivirus-based short hairpin RNAs or AS4583 treatment. (A) Cell survival decreases after MCM2 knockdown. The cells were infected with the indicated lentivirus in medium containing polybrene (8 μg/ml). At 24 h post-infection, the cells were transferred to fresh medium and incubated for 48 h, then analyzed by immunoblotting and the sulforhodamine B assay. (B)MCM2 knockdown decreases cell survival in a dose-dependent manner. The cells were infected with the indicated lentivirus in medium containing polybrene (8 μg/ml). At 24 h post-infection, the cells were incubated in fresh medium lacking lentivirus and polybrene for 48 h and analyzed with the MTS assay over an additional 24 to 120 h. (C) Cellular levels of MCM2 were detected in different lung-cancer cells as assessed with immunoblotting. (D) Quantification of MCM2 levels and IC_{50} values for each cell line were used to calculate the correlation between the two cofactors in these different lung-cancer cell lines (IC_{50} versus MCM2, R^2= 0.5282).

High expression of the MCM complex is associated with poor clinical outcomes of NSCLC patients

To further validate whether the MCM complex is a potential therapeutic target for NSCLC, we examined the cellular levels of MCM components by analyzing the gene expression data obtained from 226 pathological stage I and II lung adenocarcinomas in the public database GSE31210[20]. The results indicated that high expression of MCM2, MCM4, MCM5, or MCM6 is associated with poor overall survival compared with the low-expression group (Figure 4). Thus, the components of the MCM complex may serve as markers for high-risk patients and as potential therapeutic targets for the treatment of early stage lung adenocarcinoma.

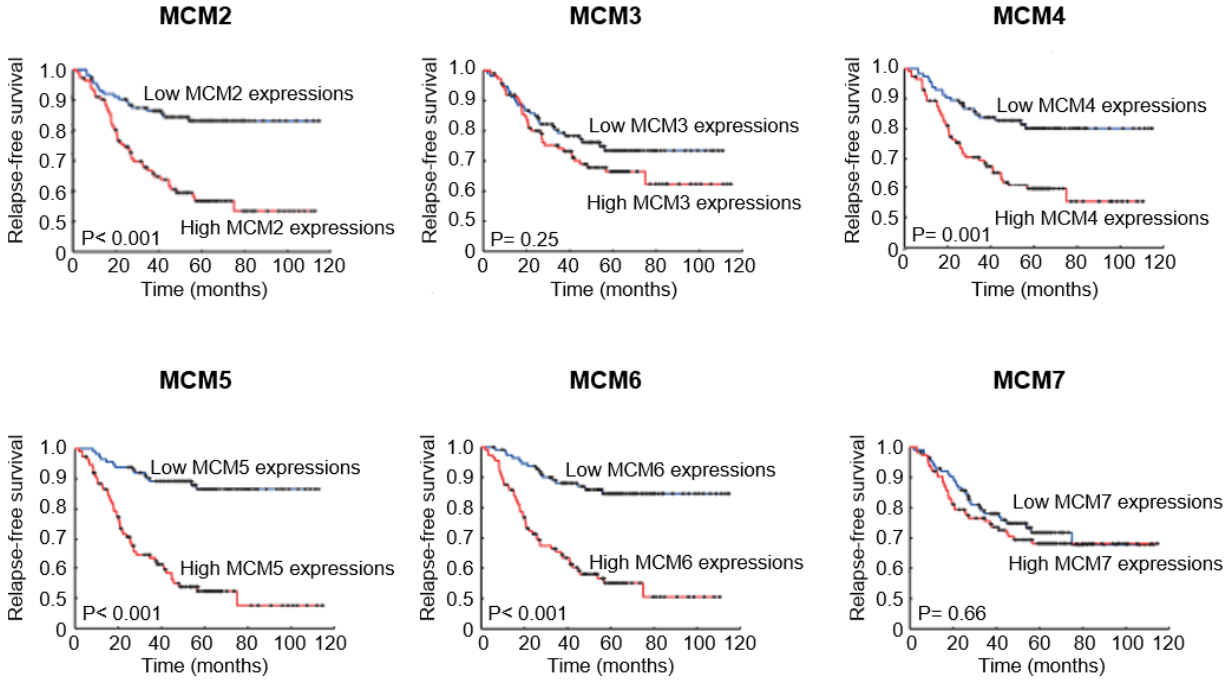

Figure 4. Clinical significance and prognostic value of MCM in NSCLC. Kaplan-Meier analysis of MCM expression and overall survival for 226 human lung adenocarcinoma samples, pathological stage I or II, published as GSE31210. The p-values were obtained with a two-sided log-rank test.

AS4583 promotes ubiquitination of MCM2–7 and their degradation in lung-cancer cells

The hetero-hexametric MCM2-7 protein complex has been identified as an important component for the precisely coordinated replication of the entire genome each time a cell divides[21]. We next determined whether AS4583 treatment could modulate the expression of MCM protein components. As expected, the cellular levels of MCM2, MCM6, and MCM7 decreased significantly (Figure 5A) in an AS4583 dose–dependent manner (Figure 5B) at 24 h after treatment, whereas the levels of MCM3, MCM4 and MCM5 decreased after 72 h (Figure 5A). This decrease in MCM expression appeared to be a consequence at the protein level because the levels of the corresponding mRNAs did not change over the course of AS4583 treatment (Supplementary Figure 2). In support of this idea, the observed decrease in MCM2, MCM6, and MCM7 was abrogated after treatment with the proteasome inhibitor MG132 (Figure 5C). Indeed, the MCM2 levels in H1975 cells were almost completely restored to the control level by MG132, whereas partial restoration was observed for MCM6 and MCM7. Further experiments confirmed that ubiquitination of MCM2 increased in the presence of AS4583 (Figure 5D).

To explore whether the AS4583-induced MCM protein degradation was due to interfere with the DNA binding ability of MCM2, H1975 cells were synchronized using a double thymidine block followed by release and subsequent treatment with DMSO (control) or AS4583 for 9 h. Then, the chromatin-bound MCM2 was detected by immunoblotting. As shown in Figure 5E, temporal binding of MCM2 to chromatin was observed in DMSO-treated cells. The bound MCM2 level decreased at 4.5 h after release from the block and later returned to the pre-block level. In the AS4583-treated group, the dynamic binding was not observed; instead, the level of MCM2 decreased significantly during the course of treatment. Moreover, we also observed that AS4583 induced-MCM2 degradation could be restored upon treatment of cells with the cullin inhibitor MLN4924 (Figure 5F), which is consistent with the fact that

MCM2/3/5/6/7 have been identified as substrates of cullin-RING ligases[22]. Collectively, all these suggest that MCM2 might be the therapeutic target of AS4583 treatment.

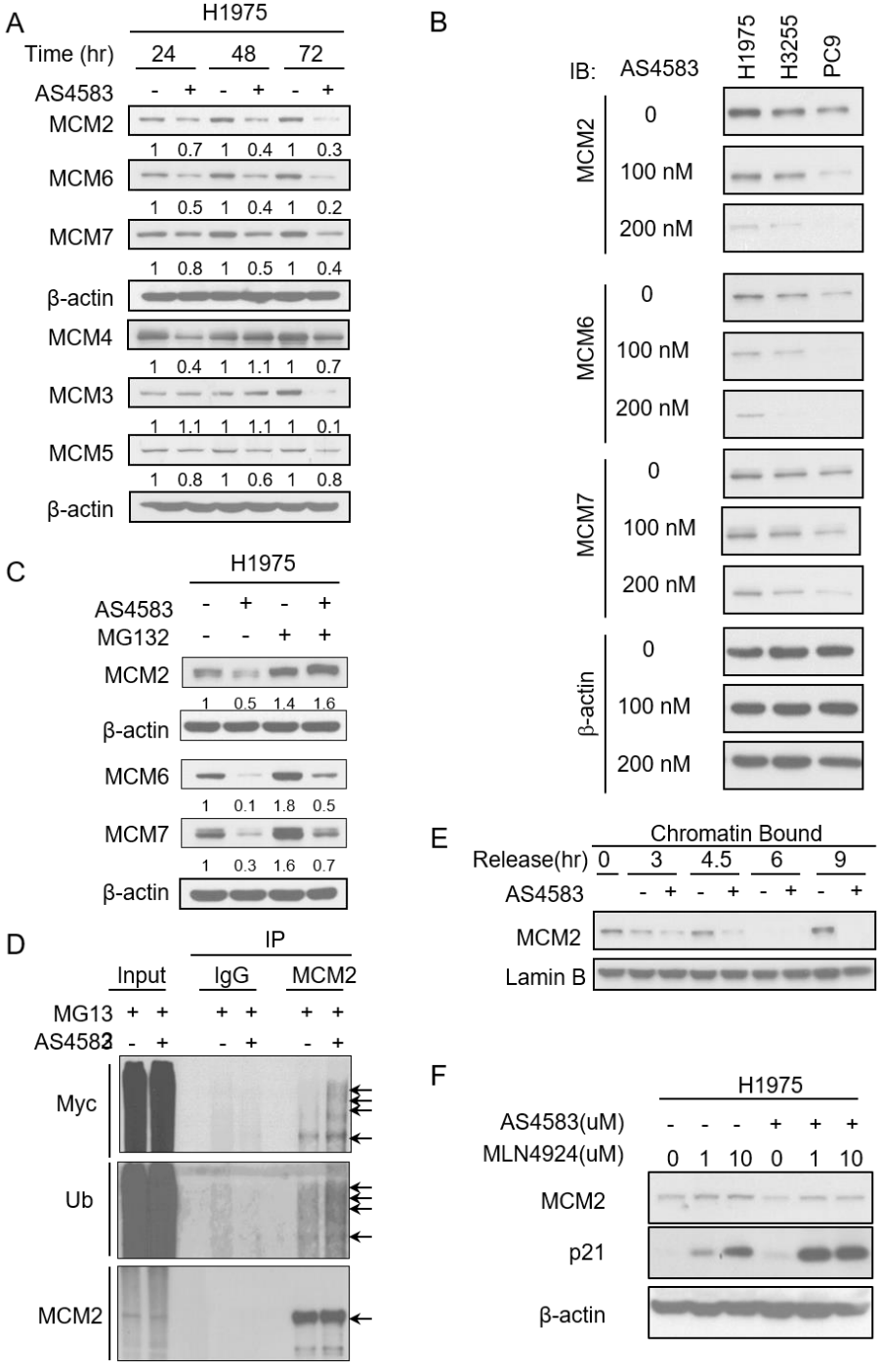

Figure 5. AS4583 induces proteasome-mediated degradation of MCM2 after loss chromatin bound ability. (A) Increased degradation of MCM2/6/7 upon treatment of H1975 cells with AS4583. AS4583-treated cells were harvested at 24, 48, and 72 h, and the levels of proteins of the MCM complex were analyzed with immunoblotting. (B) Dose-dependent degradation of MCM2/6/7 in different lung cancer cell lines. All cells were treated with AS4583 for 24 h and then harvested. The levels of MCM2/6/7 were examined with immunoblotting. (C) The proteasome inhibitor MG132 reverses the effects of AS4583 on the cellular levels

of MCM2/6/7. H1975 cells were treated with AS4583 for 48 h, then incubated in the absence or presence of MG132 (10 μM) for an additional 12 h, and then harvested. The levels of MCM2/6/7 were examined with immunoblotting. (D) AS4583 induces ubiquitination of MCM2. The cells were transiently transfected with pcDNA3-Myc-Ub and then incubated in the absence or presence of AS4583 (140 nM) and MG132 (10 μM). After 12 h, the cells were harvested, and MCM2 was precipitated with an MCM2-specific antibody. Ubiquitination of MCM2 was detected with immunoblotting. IgG served as the antibody negative control for the immunoprecipitation (IP) experiment. (E) Treatment with AS4583 decreases the level of the chromatin-bound form of MCM2. A double thymidine block was performed, and the data were collected at the indicated time points. (F)MCM2 protein levels were recovered upon treatment of H1975 cells with MLN4924. Cells were treated with DMSO or AS4583 for 24 h, and then co-treated with different dose of MLN4924. After 6 h, the cells were harvested for detection of MCM2.

AS4583 binds the N-terminal portion of MCM2

Our results thus far raised an important question: does AS4583 bind directly to MCM2? To address this issue, we incubated H1975 lysates with AS4583-conjugated magnetic beads (Figure 6A) for 24 h at 4 °C, and the results showed that more MCM2 was pulled down by the mag-beads-AS4583 compared with the mag-beads-control (Figure 6B). In addition, we also performed an *in silico* modeling and simulation to provide structural insights into the binding of AS4583 to MCM2 (Supplementary Results and Supplementary Figure 3-5). We modelled the MCM2 structure based on the crystal structure of an archaeal MCM from *Sulfolobus solfataricus* (ssoMCM, PDB: 3F9V). Although the amino acid sequence identity of MCM2 to ssoMCM is only 38%, the confidence estimate of the fold recognition server is 100%, suggesting this template used for the homology modeling is highly reliable. The final structure of MCM2 was optimized by molecular dynamics procedure, and the validation results revealed that our model structure is of good quality for further studies. The protein-ligand docking program iGEMDOCK predicted that the binding site for AS4583 is in the N-terminal domain of MCM2. This site resides within a cavity surrounded by domains A, B and C (Figure 6C and D). The solvent-accessible portion of the binding site is close to the interface between MCM2 and MCM6 in the MCM hexamer (Figure 6E). The B domain of MCM6 may rotate and insert into this site, thereby promoting the interaction with MCM2. The predicted binding energy is –8.8 kcal/mol for AS4583 in complex with MCM2 (Figure 6F); and residues from the three domains, including His282 and Gln257 in domain A, Gln341 in domain B, and

Asn442 in domain C, are involved in the AS4583 interaction. In particular, Gln341 contributes substantially to the intermolecular hydrogen-bond formation.

To validate the *in silico* docking results concerning Gln341, we constructed the plasmids p3xFlag-MCM2-WT and p3xFlag-MCM2-Q341A for overexpression in H1975 cells. The western blotting analysis of MCM2-WT or MCM2-Q341A cells shows that Flag-tagged protein expressed. The magnetic-bead pulldown assay revealed significantly less binding of MCM2-Q341A to mag-beads-AS4583 compared with the binding of the control, Flag-tagged MCM2-WT (Figure 6G). Next, we investigated that if MCM2 MCM2-Q341A can serve as a resistant clone by testing IC_{50} of AS4583 and ubiquitination of MCM2. The IC_{50} of AS4583 is 71nM for MCM2-WT cells and 150nM for MCM2-Q341A cells (Supplementary Figure 6A). We also performed the immunoprecipitation assay to pull down Flag-tagged MCM2-WT or -Q341A with AS4583 treatment for 24 hours and then detected the polyubiquitinated species of MCM2 by immunoblotting. In accordance with the previous result, treatment with AS4583 significantly enhanced the ubiquitination of MCM2-WT, but reduced ubiquitination of MCM2-Q341A in 293T cells (Supplementary Figure 6B). These data indicate that Q341A weakened the cytotoxicity and proteasomal-dependent ubiquitination of AS4583. This result supports the critical contribution of Gln341 for binding of AS4583 to MCM2.

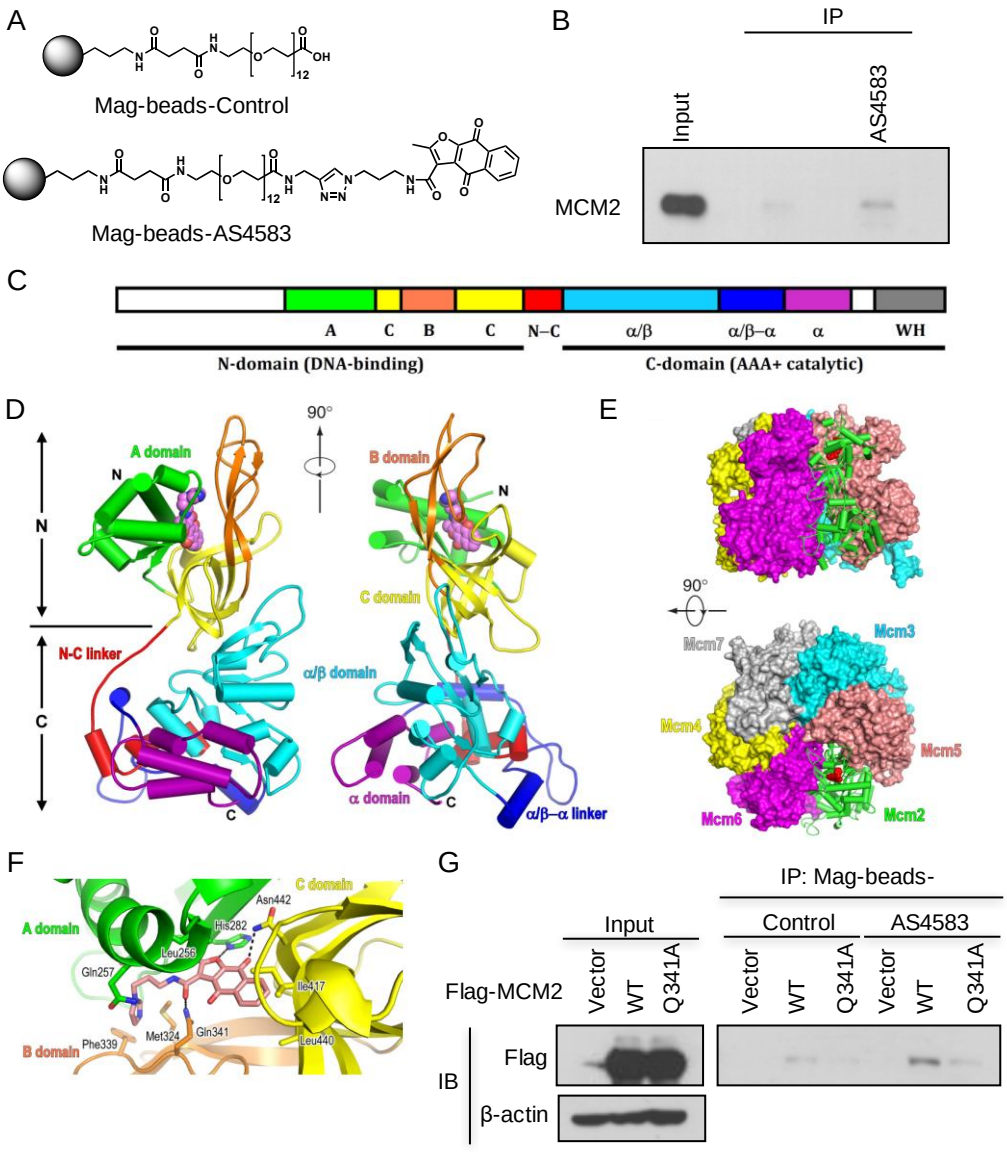

Figure 6. The interaction between AS4583 and MCM2. (A) Structure of mag-beads-control and mag-beads-AS4583. (B) AS4583 binds MCM2. H1975 cell lysates were incubated with magnetic beads-control or magnetic beads-AS4583 overnight, and the bound MCM2 proteins were detected with immunoblotting. (C) Domain organization of MCM2. N-C, N to C linker; α/β, α/β domain of the AAA+ ATPase core structure; α/β-α, linker between subdomains in the ATPase core; α, α domain; WH, winged-helix domain. The domain annotation is based on the structure of *Sulfolobus solfataricus* (ssoMCM, PDB: 3F9V). (D) Model for MCM2 complexed with AS4583. Domains and linkers have the same coloring as depicted in panel c. Helices are depicted as cylinders and β-strands as arrows. The AS4583 structure is shown as a space-filling model (pink, carbon; blue, nitrogen; red, oxygen). (E) Model of AS4583 in the MCM hexamer. Protomers (MCM2–7) are colored differently and labeled. AS4583 is shown as red spheres. (F) The AS4583 binding pocket. The domains have the same coloring as in panel c. The residues involved in AS4583 binding are shown as stick structures. The black dashed lines represent polar contacts between amino acid residues and AS4583. (G) Mag-beads-AS4583 pulled down less MCM2 Q341A than MCM2 wild type. Immunoprecipitation (IP) was performed by incubating lysates of cells that overexpressed FLAG, FLAG-MCM2 wild-type, or the Q341A mutant with mag-beads-control or -AS4583.

Cell-based SAR study of AS4583 reveals essential molecular functionality of AS4583 that mediates the inhibition of H1975 cell proliferation

To identify the structural components of AS4583 that are essential for its ability to inhibit the proliferation of lung-cancer cells, a preliminary SAR study was carried out with modifications of the X, R1 and R2 groups of AS4583 in Table 1 and the length (n) of the side chain on the furan ring. The ability of each analog to inhibit H1975 cell proliferation was evaluated using the sulforhodamine B assay. As shown in Table 1, analogs with different amide side-chain lengths (compound 1, n=0, and compound 2, n=2) and R^1 group sizes (compound **3**-**5**) suppressed H1975 cell proliferation with IC_{50} of <1.0 μM. The IC_{50} value of the pyrrole analog **6** was 100-fold higher than that of AS4583, and benzofuran **11** had little or no effect up to 10 μM. These results suggested that both the furan oxygen and benzoquinone moiety are essential for AS4583 activity. Replacement of the imidazole group at the end of the amide chain of AS4583 with morpholine (compound 8) did not affect the IC_{50} value (80 nM), and compound **10**, with a benzyl tail end, was unable to suppress H1975 cell proliferation even at a dose of 10 μM. These results indicated that the tertiary nitrogen of the amide chain is essential for the anti-proliferation activity of AS4583. Notably, compound **9**, with a pyrrolidine moiety instead of an imidazole ring, had the best activity with IC_{50} 24 nM, while the activity was diminished with pyrrolyl side chain (**7**, IC_{50} 918 nM). According to the SAR study (Table 1), the furan oxygen is important for AS4583 activity. This finding is coherent with our predicted binding model (Figure 6F), because the furan oxygen forms a hydrogen bond with His282 sidechain. The size of R1 moiety is also closely related to AS4583 activity. In our predicted binding model, the R1 methyl moiety is surrounded by Ile281, Val283 and Leu256, and therefore a much bulky moiety cannot fit into this pocket. In addition, the replacement of R1 by a proton would reduce the van der Waals force for the AS4583 binding.

Table 1. SAR study of AS4583

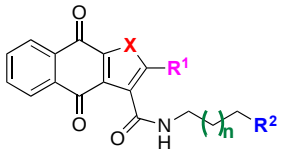

Compound	n	R1	R2	X	IC_{50} (nM)
AS4583	1	Me		O	77
1	0	Me		O	280
2	2	Me		O	250
3	1	Et		O	288
4	1	iPr		O	260
5	1	Ph		O	826
6	1	Me		NH	8727
7	1	Me		O	918
8	1	Me		O	80
9	1	Me		O	24
10	2	Me		O	>10μM
11			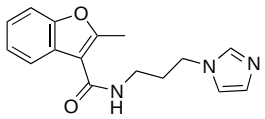		>10 μM

Synthesis of a more potent lead compound, RJ-LC-07-48

Although compound **9** was the most potent inhibitor of H1975 cell viability in the aforementioned analysis (IC_{50} 24 nM), it also exhibited toxicity toward skin fibroblast cells (Hs68, IC_{50} 77 nM). To further improve the potency of AS4583 and reduce its toxicity, a new analog, RJ-LC-07-48 was synthesized from 7-fluoro-1-tetralone (**12**). As shown in Scheme 1, 7-fluoro-1-

tetralone was regioselectively oxidized to 2-hydroxynaphthoquinone (**13**) under an oxygen atmosphere. A three-components reaction[23] was then applied to transfer compound **13** to a phosphorus zwitterion **14**. A Wittig reaction between **14** and acetyl chloride provided furanonaphthoquinone **15**, which was then hydrolyzed to acid **16** and then linked with the imidazole side chain to complete the synthesis. Fortunately, the survival assay showed that RJ-LC-07-48 had a better activity in the inhibition of H1975 cell viability (Supplementary Figure 7A, IC_{50} 17nM). In addition, treatment with RJ-LC-07-48 markedly reduced the growth of H1975 xenograft tumors in mice compared with the control group: average tumor size, 546.2 ± 95.2 mm^3 for DMSO/control, 128.2 ± 50.5 mm^3 for 1 mg/kg RJ-LC-07-48, and 109.5 ± 23.1 mm^3 for 4 mg/kg RJ-LC-07-48 on day 24; $p< 0.05$, n=6 per group, Supplementary Figure 7G). All these results suggested that RJ-LC-07-48 is a potential lead compound for treatment of lung cancer.

SCHEME 1. Stereoselective synthesis of RJ-LC-07-48

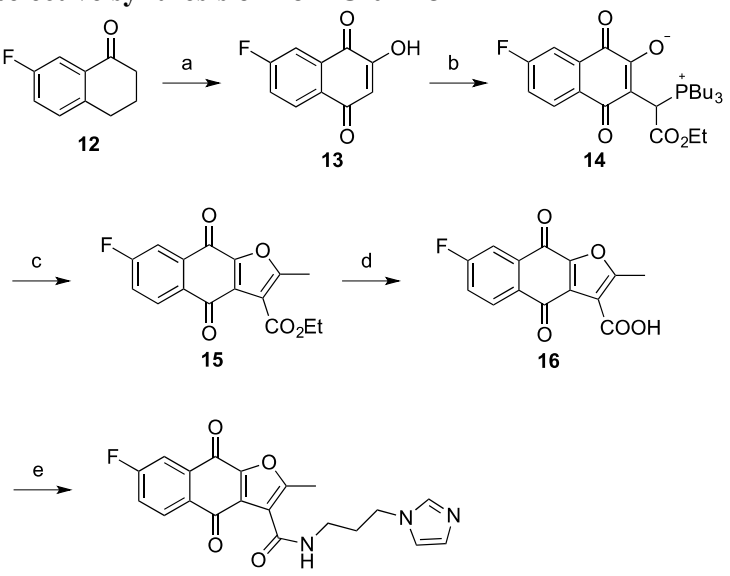

Reagents and conditions: a) O_2 atmosphere, room temperature (r.t.), 50 min, 90%; b) $CHOCO_2Et$, TFA, PBu_3, THF, 0–64 °C, 3.5 h, 63%; c) acetyl chloride, Et_3N, THF, 0 °C to r.t., 15 min, 77%; d) 3 M NaOH, THF: H_2O (4:1), 0 °C to r.t., 5 h, 97%; e) HBTU, DMAP, 1-(3-aminopropyl) imidazole, DMF, r.t., 6 h, 64%.

DISCUSSION

Through the high-throughput cell-based screening and SAR study, we have identified a furanonaphthoquinone-based small molecule, AS4583, which can induce the proteasome degradation of MCM2–7 and ultimately contribute to the death of NSCLC cells. The SAR study of AS4583 further identified the furanonaphthoquinone moiety and the tertiary nitrogen at the end of the side chain as crucial components for the inhibition of tumor growth. Through computer-simulated docking, we found that AS4583 could bind to MCM2 by forming a hydrogen bond with residue Q341, and this result was supported by immunoprecipitation experiments using anti-MCM2. Finally, a more potent compound RJ-LC-07-48 was synthesized with better antitumor effect than AS4583 *in vivo*.

We found that AS4583 contributes to the induction of ubiquitinated-MCM2, leading to degradation of MCM2 by the proteasome. MCM2 degradation may further interfere with the formation of the MCM complex, cause inhibition of DNA replication, and prolong the duration of S phase in cancer cells. MCM2 degradation may ultimately promote apoptosis *in vitro* and inhibit tumor growth *in vivo.* Since MCM2–7 must be assembled as a hexamer or tetramer before nuclear import[19, 21], the degradation of ubiquitinated MCM2 in proteasomes may interfere with the formation of the MCM complex, perturb its import into the nucleus, and inhibit chromatin loading.

The docking analysis revealed that AS4583 does not occupy the ATP binding site in the C-terminal ATPase domain of MCM2 but rather binds to the cavity in the N-terminal domain. Indeed, the N-terminal portion of MCM2 has been shown to be important for the hexamer formation, DNA binding, and enzyme regulation[24]. Mutational and biochemical analyses carried out by others have further suggested that a conformational change in the N-terminal portion (especially the movement of domain A) is required for helicase function[25, 26]. The binding of

AS4583 to MCM2 may alter the rigidity of the N-terminal portion and hinder the movement of domain A. In addition, the bound AS4583 molecule could interfere with the interaction between MCM6 and MCM2 and therefore perturb hexamer assembly and helicase function. Based on these findings, we propose a paradigm for AS4583–induced apoptosis. Cells typically progress through the cell cycle using the MCM2–7 helicases to unwind the DNA double helix for DNA replication. In cancer cells, however, the MCM2–7 complex is highly regulated through the G0-G1 to S phase. Once this complex is disrupted, the cancer cells will undergo apoptosis. As important components in the process of DNA replication for malignant proliferation, MCM2–7 represent a potential class of drug targets for lung-cancer treatment in the near future.

This is the first report to show that a small molecule can induce MCM2 ubiquitination and suppress the expression of MCM2. Although previous studies reported that norcantharidin induced the cleavage of MCM2 at the micro-molar level[27] and that MCM2 is a therapeutic target of Trichostatin A in colon cancer cells[28], their mechanisms of action remain unclear and need clarification. In addition, high expression levels of MCM complex proteins are associated with poor survival of patients with NSCLC. In summary, our results demonstrate that the MCM complex can serve as a potential target for lung-cancer treatment, and this work paves the way for development of new cancer agents to tackle the problem of drug resistance.

CONCLUSION

The use of high-throughput drug screens for various lung-cancer cells and of *in silico* docking prediction will provide effective means for identifying small molecules that target the MCM complex, which is important for developing new cancer therapeutics. Our results demonstrate that proteins of the MCM complex can serve as potential targets for lung-cancer treatment, and our SAR analysis paves the way for design of potent lead compounds.

EXPERIMENTAL SECTION

Synthesis and characterization of chemical compounds

Unless stated otherwise, reactions were performed in flame-dried glassware under a positive pressure of nitrogen. Commercial grade reagents and solvents were used without further purification. CH_2Cl_2, CH_3CN and THF were purified by PS-MD-5 solvent purification system (Innovative Technology, Inc). Magnetic bead was purchased from TAN Beads, Taiwan. The progress of all the reactions were monitored by TLC, using TLC glass plates pre-coated with silica gel 60 F_{254} (Merck). Flash column chromatography was performed with silica gel Geduran® Si 60 (Merck). IR spectra were recorded with Thermo Nicolet iS-5 FT-IR spectrophotometer, ν_{max} in cm^{-1}. ^1H and ^{13}C NMR spectra were recorded with Bruker AV-III 400 MHz or Bruker AV-400 MHz spectrometers and chemical shifts were measured in δ (ppm) with residual solvent peaks as internal standards ($CDCl_3$, δ 7.24 ppm in ^1H NMR, δ 77.0 ppm in ^{13}C NMR; CD_3OD, δ 3.31 ppm in ^1H NMR, δ 49.0 ppm in ^{13}C NMR). Coupling constants *J*, measured in Hz. HR FAB (LR FAB) and HR EI (LR EI)-mass spectra were recorded on a JMS-700 double focusing mass spectrometer (JEOL, Tokyo, Japan) with a resolution of 8000 (3000) (5 % valley definition) and HR (LR) ESI (Electrospray)-mass spectra were recorded using dual ionization ESCi® (ESI/APCi) source options, Waters LCT premier XE (Waters Corp., Manchester, UK). Melting points were recorded on Büchi M-565 apparatus. Purity of all compounds for biology test was found to be >98% as determined by HPLC (Shimadzu LCMS-2020 with Unitary C18 columns).

SCHEME 2. Synthesis of AS4583.

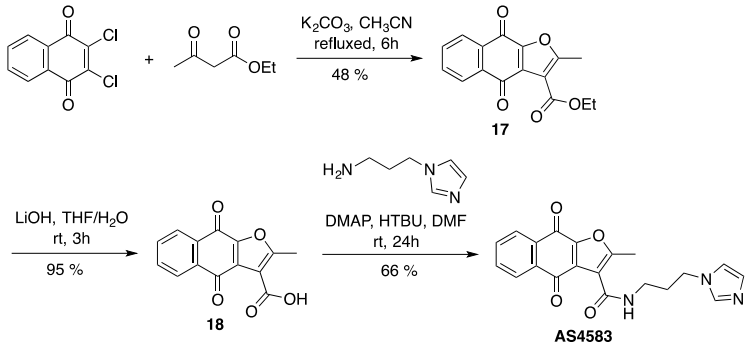

Ethyl 2-methyl-4, 9-dioxo-4, 9-dihydronaphtho [2, 3-*b*] furan-3-carboxylate (17)

A mixture of 2, 3-dichloro-1, 4-naphthoquione (500 mg, 2.20 mmol), K_2CO_3 (760 mg, 5.51 mmol) and ethyl acetoacetate (0.31 mL, 2.42 mmol) in MeCN (30 mL) was stirred at reflux temperature for 6 hr. After completion, the reaction mixture was diluted with EtOAc and filtered through Celite®, filtrate was evaporated in *vacuo* to yield the crude product. The residue was purified by flash column chromatography (EtOAc/hexanes, 1/4 to 2/3) to give **17** as a yellow solid (305 mg, 48 % yield). R_f (30 % EtOAc/hexanes) 0.52; Mp 149.3 – 159.9 °C; ^{1}H NMR (400 MHz, $CDCl_3$) δ 8.42 – 7.99 (m, 2H), 7.98 – 7.53 (m, 2H), 4.43 (q, J = 7.2 Hz, 2H), 2.70 (s, 3H), 1.43 (t, J = 7.1 Hz, 3H); ^{13}C NMR (100 MHz, $CDCl_3$) δ 178.7, 173.5, 164.4, 162.0, 151.3, 134.1, 133.7, 133.6, 131.5, 128.2, 127.4, 126.5, 113.8, 61.5, 14.2, 14.2.

2-Methyl-4, 9-dioxo-4, 9-dihydronaphtho [2, 3-*b*] furan-3-carboxylic acid (18)

To a stirred solution of **17** (378 mg, 1.33 mmol) in THF/H_2O (0.2 M, 7/3 v/v) was added LiOH (167 mg, 3.99 mmol) at room temperature. After stirred at room temperature for 3 hr, the reaction mixture was quenched with 1N HCl (adjust to pH ~ 1, aqueous layer will show transparent), extracted with EtOAc (15 mL x 3), dried over Na_2SO_4, and concentrated in *vacuo*. The residue was purified by flash column chromatography (MeOH/CH_2Cl_2, 0/100 to 1/9) to give **18** as a yellow

solid (324 mg, 95 % yield). R_f (5 % MeOH/CH_2Cl_2) 0.35; IR (neat) 3425, 3022, 2975, 2920, 2712, 1744, 1673, 1581, 1413, 1217, 1192, 995, 721 cm^{-1}; ^1H NMR (400 MHz, $CDCl_3$) δ 8.25 (td, J = 7.4, 1.2 Hz, 2H), 7.84 (dtd, J = 18.8, 7.5, 1.3 Hz, 2H), 2.88 (s, 3H); ^{13}C NMR (100 MHz, $CDCl_3$) δ 184.9, 172.4, 169.0, 160.9, 150.9, 135.8, 134.5, 131.8, 131.7, 128.0, 127.5, 126.0, 112.8, 14.5.

_N_-(3-(1_H_-Imidazol-1-yl) propyl)-2-methyl-4, 9-dioxo-4, 9-dihydronaphtho [2, 3-_b_] furan-3-carboxamide (AS4583)

To a stirred solution of **18** (256.2 mg, 1.0 mmol), DMAP (12.2 mg, 0.1 mmol) and HBTU (455 mg, 1.2 mmol) in DMF (5 mL) was added 1-(3-Aminopropyl) imidazole (180 μL, 1.5 mmol) at room temperature. The solvent was removed by *vacuo* after the reaction mixture was stirred at room temperature for 1 day. Then the crude was washed by H_2O, extracted with CH_2Cl_2 (10 mL x 3), dried over Na_2SO_4, and concentrated in *vacuo*. The residue was purified by flash column chromatography (MeOH/CH_2Cl_2, 0/100 to 1/49) to give **AS4583** as a yellow solid (240 mg, 66 % yield). R_f (5 % MeOH/CH_2Cl_2) 0.28; IR (neat) 3285, 3095, 2923, 2848, 1650, 1582, 1213, 991, 844, 715 cm^{-1}; ^1H NMR (400 MHz, $CDCl_3$) δ 9.79 (s, 1H), 8.21 (qd, J = 4.0, 1.7 Hz, 2H), 7.83 – 7.76 (m, 2H), 7.59 (s, 1H), 7.07 (s, 1H), 7.00 (s, 1H), 4.11 (t, J = 7.0 Hz, 2H), 3.46 (dd, J = 12.5, 6.2 Hz, 2H), 2.87 (s, 3H), 2.16 (quint, J = 6.8 Hz, 2H); ^{13}C NMR (100 MHz, $CDCl_3$) δ 183.3, 172.9, 166.5, 161.5, 151.1, 137.2, 134.8, 134.2, 132.7, 131.4, 129.3, 127.8, 126.9, 125.9, 118.9, 115.1, 44.5, 36.2, 30.9, 14.9; HRMS (ESI^+, TOF) calcd for $C_{20}H_{18}N_3O_4$ $[M + H]^+$ 364.1297, found 364.1289.

***N*-(2-(1*H*-imidazol-1-yl)ethyl)-2-methyl-4, 9-dioxo-4, 9-dihydronaphtho [2, 3-*b*]furan-3-carboxamide (1)**

To a stirred solution of **18** (0.17 mmol), DMAP (21 mg, 0.17 mmol) and HBTU (97 mg, 0.26 mmol) in DMF (0.85 mL) was added 2-Imidazol-1yl-ethylamine (47 mg, 0.43 mmol) at room temperature. The solvent was removed by *vacuo* after the reaction mixture was stirred at room temperature for 1 day. Then the crude was washed by H_2O, extracted with CH_2Cl_2 (10 mL x 3), dried over Na_2SO_4, and concentrated in *vacuo*. The residue was purified by flash column chromatography (MeOH/CH_2Cl_2, 0/100 to 1/49) to give **1** as a yellow solid (42 mg, 70 % yield). Rf (5 % MeOH/CH_2Cl_2) 0.28; ^{1}H NMR (400 MHz, CD_3OD) δ 8.27 – 8.14 (m, 3H), 7.92 – 7.81 (m, 2H), 7.43 (s, 1H), 7.22 (s, 1H), 4.41 (t, J = 6.0 Hz, 1H), 3.86 (t, J = 6.0 Hz, 1H), 2.77 (s, 3H); ^{13}C NMR (100 MHz, CD_3OD) δ 184.0, 174.2, 167.1, 163.7, 152.6, 138.8, 135.9, 135.4, 134.2, 132.9, 129.3, 128.6, 127.5, 127.2, 120.8, 115.8, 47.2, 41.3 14.7; HRMS (ESI^+, TOF) calcd for $C_{19}H_{16}N_3O_4$ $[M + H]^+$ 350.1141, found 350.1135. Sample for biology test was purified by preparative HPLC with HPLC purity >99%.

***N*-(4-(1*H*-imidazol-1-yl)butyl)-2-methyl-4,9-dioxo-4,9-dihydronaphtho[2,3-*b*]furan-3-carboxamide (2)**

To a stirred solution of **18** (95 mg, 0.37 mmol), DMAP (45 mg, 0.37 mmol) and HBTU (154 mg, 0.41 mmol) in DMF (1.9 mL) was added 4-(1*H*-imidazol-1-yl) butan-1-amine (77 mg, 0.56 mmol) at room temperature. The solvent was removed by *vacuo* after the reaction mixture was stirred at room temperature for 18 hr. Then the crude was washed by H_2O, extracted with CH_2Cl_2 (10 mL x 3), dried over Na_2SO_4, and concentrated in *vacuo*. The residue was purified by flash column chromatography (MeOH/CH_2Cl_2, 0/100 to 1/49) to give **2** as a yellow solid (97 mg, 70 % yield). Rf (5 % MeOH/CH_2Cl_2) 0.25; mp 158.6 – 164.1 °C; ^{1}H NMR (400 MHz, $CDCl_3$) δ 9.70 (s, 1H), 8.18 (d, J = 7.5 Hz, 2H), 7.83 – 7.75 (m, 2H), 7.49 (s, 1H), 7.03 (s, 1H), 6.93 (s, 1H),

4.01 (t, *J* = 7.1 Hz, 2H), 3.47 (dd, *J* = 12.6, 6.4 Hz, 2H), 2.86 (s, 3H), 1.94 (dt, *J* = 15.1, 7.4 Hz, 2H), 1.69 (dt, *J* = 14.2, 6.9 Hz, 2H); ^{13}C NMR (100 MHz, $CDCl_3$) δ 183.1, 172.8, 166.4, 161.3, 151.0, 137.0, 134.7, 134.1, 132.7, 131.4, 129.3, 127.6, 126.7, 125.9, 118.7, 115.2, 46.6, 38.5, 28.5, 26.4, 14.9; HRMS (ESI$^+$, TOF) calcd for $C_{21}H_{20}N_3O_4$ $[M + H]^+$ 378.1454, found 378.1448. Sample for biology test was purified by preparative HPLC with HPLC purity >99%.

_N_-(3-(1_H_-imidazol-1-yl)propyl)-2-ethyl-4,9-dioxo-4,9-dihydronaphtho[2,3-_b_]furan-3-carboxamide (3)

To a stirred solution of 2-ethyl-4,9-dioxo-4,9-dihydronaphtho[2,3-*b*]furan-3-carboxylic acid (92 mg, 0.34 mmol), DMAP (42 mg, 0.34 mmol) and HBTU (142 mg, 0.37 mmol) in DMF (1.7 mL) was added 1-(3-Aminopropyl)imidazole (49 μL, 0.41 mmol) at room temperature. The solvent was removed by *vacuo* after the reaction mixture was stirred at room temperature for 1 day. Then the crude was washed by H_2O, extracted with CH_2Cl_2 (10 mL x 3), dried over Na_2SO_4, and concentrated in *vacuo*. The residue was purified by flash column chromatography (MeOH/CH_2Cl_2, 0/100 to 1/19) to give **3** as a yellow solid (116 mg, 90 % yield). Rf (5 % MeOH/CH_2Cl_2) 0.31; ^{1}H NMR (400 MHz, $CDCl_3$) δ 9.82 (s, 1H), 8.26 – 8.18 (m, 2H), 7.84 – 7.74 (m, 2H), 7.66 (s, 1H), 7.08 (s, 1H), 7.02 (s, 1H), 4.12 (t, *J* = 7.0 Hz, 2H), 3.46 (dd, *J* = 12.5, 6.2 Hz, 2H), 3.35 (q, *J* = 7.5 Hz, 2H), 2.24 – 2.10 (m, 2H), 1.36 (t, *J* = 7.5 Hz, 3H); ^{13}C NMR (100 MHz, $CDCl_3$) δ 183.5, 173.0, 171.2, 161.5, 151.3, 137.3, 134.8, 134.2, 132.8, 131.6, 129.5, 127.8, 126.9, 118.9, 114.4, 44.6, 36.3, 31.0, 22.1, 12.0; HRMS (MALDI$^+$, TOF) calcd for $C_{21}H_{20}N_3O_4$ $[M + H]^+$ 378.1448, found 378.1457. Sample for biology test was purified by preparative HPLC with HPLC purity >99%.

_N_-(3-(1_H_-imidazol-1-yl)propyl)-2-isopropyl-4,9-dioxo-4,9-dihydronaphtho[2,3-_b_]furan-3-carboxamide (4)

To a stirred solution of 2-isopropyl-4,9-dioxo-4,9-dihydronaphtho[2,3-*b*]furan-3-carboxylic acid (41.8 mg, 0.15 mmol), DMAP (18 mg, 0.15 mmol) and HBTU (61 mg, 0.16 mmol) in DMF (0.74 mL) was added 1-(3-Aminopropyl)imidazole (21 μL, 0.18 mmol) at room temperature. The solvent was removed by *vacuo* after the reaction mixture was stirred at room temperature for 1 day. Then the crude was washed by H_2O, extracted with CH_2Cl_2 (10 mL x 3), dried over Na_2SO_4, and concentrated in *vacuo*. The residue was purified by flash column chromatography (MeOH/CH_2Cl_2, 1/199 to 1/19) to give **4** as a yellow solid (52 mg, 90 % yield). Rf (5 % MeOH/CH_2Cl_2) 0.32; ^{1}H NMR (400 MHz, $CDCl_3$) δ 9.83 (s, 1H), 8.20 (td, *J* = 5.3, 1.8 Hz, 2H), 7.83 – 7.73 (m, 2H), 7.72 (s, 1H), 7.08 (s, 1H), 7.05 (s, 1H), 4.34 – 4.27 (m, 1H), 4.14 (t, *J* = 7.0 Hz, 2H), 3.46 (dd, *J* = 12.4, 6.2 Hz, 2H), 2.17 (quint, *J* = 6.8 Hz, 2H), 1.37 (s, 3H), 1.36 (s, 3H); ^{13}C NMR (100 MHz, $CDCl_3$) δ 183.6, 174.1, 172.9, 161.6, 151.3, 134.8, 134.2, 132.8, 131.6, 128.7, 127.7, 126.8, 125.9, 113.5, 44.8, 36.2, 30.9, 27.7, 20.4; HRMS (ESI^+, TOF) calcd for $C_{22}H_{22}N_3O_4$ $[M + H]^+$ 392.1610, found 392.1605. Sample for biology test was purified by preparative HPLC with HPLC purity >98%.

_N_-(3-(1_H_-imidazol-1-yl)propyl)-4,9-dioxo-2-phenyl-4,9-dihydronaphtho[2,3-_b_]furan-3-carboxamide (5)

To a stirred solution of 4,9-dioxo-2-phenyl-4,9-dihydronaphtho[2,3-*b*]furan-3-carboxylic acid (50.9 mg, 0.16 mmol), DMAP (19.5 mg, 0.16 mmol) and HBTU (73 mg, 0.19 mmol) in DMF (0.8 mL) was added 1-(3-Aminopropyl)imidazole (29 μL, 0.24 mmol) at room temperature. The solvent was removed by *vacuo* after the reaction mixture was stirred at room temperature for 1

day. Then the crude was washed by H_2O, extracted with CH_2Cl_2 (10 mL x 3), dried over Na_2SO_4, and concentrated in *vacuo*. The residue was purified by flash column chromatography (MeOH/CH_2Cl_2, 0/100 to 1/19) to give **5** as a yellow solid (38 mg, 56 % yield). Rf (5 % MeOH/CH_2Cl_2) 0.32; ^{1}H NMR (400 MHz, $CDCl_3$) δ 9.22 (s, 1H), 8.26 – 8.22 (m, 1H), 8.12 – 8.10 (m, 1H), 7.92 – 7.89 (m, 2H), 7.84 – 7.80 (m, 2H), 7.62 (s, 1H), 7.50 – 7.44 (m, 3H), 7.06 (s, 1H), 7.01 (s, 1H), 4.14 (t, J = 7.0 Hz, 2H), 3.48 (dd, J = 12.5, 6.3 Hz, 2H), 2.18 (quint, J = 6.8 Hz, 2H); HRMS (ESI$^+$, TOF) calcd for $C_{25}H_{20}N_3O_4$ $[M + H]^+$ 426.1454, found 426.1451. Sample for biology test was purified by preparative HPLC with HPLC purity >99%.

***N*-(3-(1*H*-imidazol-1-yl)propyl)-2-methyl-4,9-dioxo-4,9-dihydro-1*H*-benzo[*f*]indole-3-carboxamide (6)**

To a stirred solution of 2-methyl-4,9-dioxo-4,9-dihydro-1*H*-benzo[*f*]indole-3-carboxylic acid (23 mg, 0.09 mmol), DMAP (17 mg, 0.14 mmol) and HBTU (51 mg, 0.14 mmol) in DMF (0.45 mL) was added 1-(3-Aminopropyl)imidazole (13 μL, 0.11 mmol) at 0 °C. The solvent was removed by *vacuo* after the reaction mixture was stirred at room temperature for 2 days. The residue was purified by flash column chromatography to give **6** as a yellow solid (9.1 mg, 28 % yield). Rf (5 % MeOH/CH_2Cl_2) 0.20; ^{1}H NMR (400 MHz, $CDCl_3$) δ 10.33 (t, J = 5.4 Hz, 1H), 8.24 – 8.10 (m, 1H), 8.10 – 7.98 (m, 1H), 7.75 – 7.63 (m, 2H), 7.60 (s, 1H), 7.00 (s, 1H), 6.99 (s, 1H), 4.10 (t, J = 7.1 Hz, 2H), 3.47 (q, J = 6.1 Hz, 2H), 2.67 (s, 3H), 2.17 – 2.05 (m, 2H); HRMS (ESI$^+$, TOF) calcd for $C_{20}H_{19}N_4O_3$ $[M + H]^+$ 363.1457, found 363.1454. Sample for biology test was purified by preparative HPLC with HPLC purity >99%.

_N_-(3-(1_H_-pyrrol-1-yl)propyl)-2-methyl-4,9-dioxo-4,9-dihydronaphtho[2,3-_b_]furan-3-carboxamide (7)

To a stirred solution of **18** (100 mg, 0.39 mmol), DMAP (47 mg, 0.39 mmol) and HBTU (163 mg, 0.43 mmol) in DMF (1.95 mL) was added 3-(1*H*-pyrrol-1-yl)propan-1-amine (58 mg, 0.47 mmol) at room temperature. The solvent was removed by *vacuo* after the reaction mixture was stirred at room temperature for 1 day. Then the crude was washed by H_2O, extracted with CH_2Cl_2 (10 mL x 3), dried over Na_2SO_4, and concentrated in *vacuo*. The residue was purified by flash column chromatography (MeOH/CH_2Cl_2, 0/100 to 1/49) to give **7** as a yellow solid (67 mg, 47 % yield). Rf (CH_2Cl_2) 0.07; Mp 143.5 – 150.7 ºC; ^{1}H NMR (400 MHz, $CDCl_3$) δ 9.73 (s, 1H), 8.26 – 8.13 (m, 2H), 7.84 – 7.71 (m, 2H), 6.74 (t, *J* = 2.1 Hz, 2H), 6.14 (t, *J* = 2.1 Hz, 2H), 4.05 (t, *J* = 6.9 Hz, 2H), 3.42 (dd, *J* = 12.3, 6.6 Hz, 2H), 2.86 (s, 3H), 2.14 (quint, *J* = 6.8 Hz, 2H); ^{13}C NMR (100 MHz, $CDCl_3$) δ 183.1, 172.9, 166.5, 161.3, 151.0, 134.7, 134.1, 132.8, 131.5, 127.7, 126.8, 126.0, 120.6, 115.3, 108.2, 47.0, 36.6, 31.2, 14.9; HRMS (MALDI$^+$, TOF) calcd for $C_{21}H_{19}N_2O_4$ $[M + H]^+$ 363.1339, found 363.1325. Sample for biology test was purified by preparative HPLC with HPLC purity >99%.

2-Methyl-_N_-(3-morpholinopropyl)-4,9-dioxo-4,9-dihydronaphtho[2,3-_b_]furan-3-carboxamide (8)

To a stirred solution of **18** (23.8 mg, 0.093 mmol), DMAP (17 mg, 0.14 mmol) and HBTU (54 mg, 0.14 mmol) in DMF (0.47 mL) was added 3-morpholinopropylamine (20.4 μL, 0.14 mmol) at 0 °C. The solvent was removed by *vacuo* after the reaction mixture was stirred at room temperature for 2 days. The residue was purified by flash column chromatography (MeOH/CH_2Cl_2, 0/100 to 1/9) to give **8** as a yellow solid. ^{1}H NMR (400 MHz, $CDCl_3$) δ 9.69 (s, 1H), 8.26 – 8.14

(m, 2H), 7.83 – 7.71 (m, 2H), 3.81 – 3.66 (m, 4H), 3.51 (dd, *J* = 12.5, 6.8 Hz, 2H), 2.87 (s, 3H), 2.60 – 2.43 (m, 6H), 1.88 (quint, *J* = 7.2 Hz, 2H); HRMS (ESI^+, TOF) calcd for $C_{21}H_{23}N_2O_5$ $[M + H]^+$ 383.1607, found 383.1604. Sample for biology test was purified by preparative HPLC with HPLC purity >99%.

2-Methyl-4,9-dioxo-*N*-(3-(pyrrolidin-1-yl)propyl)-4,9-dihydronaphtho[2,3-*b*]furan-3-carboxamide (9)

To a stirred solution of **18** (80 mg, 0.31 mmol), DMAP (57 mg, 0.47 mmol) and HBTU (177 mg, 0.47 mmol) in DMF (1.6 mL) was added 1-(3-aminopropyl)pyrrolidine (59 μL, 0.60 mmol) at 0 °C. The solvent was removed by *vacuo* after the reaction mixture was stirred at room temperature for 36 hr. The residue was purified by flash column chromatography (MeOH/EtOAc/CH_2Cl_2, 0/1/1 to 1/4/5) to give **9** as a yellow solid (47 mg, 41 % yield). ^1H NMR (400 MHz, $CDCl_3$) δ 9.72 (s, 1H), 8.20 – 8.18 (m, 2H), 7.84 – 7.68 (m, 2H), 3.51 (dd, *J* = 12.5, 6.7 Hz, 2H), 2.86 (s, 3H), 2.66 (t, *J* = 7.6 Hz, 2H), 2.62 (brs, 4H), 1.96 – 1.86 (m, 2H); 1.81 (brs, 4H); HRMS (ESI^+, TOF) calcd for $C_{21}H_{23}N_2O_4$ $[M + H]^+$ 367.1658, found 367.1657. Sample for biology test was purified by preparative HPLC with HPLC purity >99%.

2-Methyl-4,9-dioxo-*N*-(4-phenylbutyl)-4,9-dihydronaphtho[2,3-*b*] furan-3-carboxamide (10)

To a stirred solution of **18** (90 mg, 0.35 mmol), DMAP (43 mg, 0.35 mmol) and HBTU (146 mg, 0.39 mmol) in DMF (1.8 mL) was added 4-phenylbutylamine (72 μL, 0.46 mmol) at 0 °C. The solvent was removed by *vacuo* after the reaction mixture was stirred at room temperature for 20 hr. The residue was purified by flash column chromatography (EtOAc/hexanes, 1/49 to 1/9) to give **10** as a yellow solid (78 mg, 58 % yield). Rf (20 % EtOAc/hexanes) 0.35; mp 151.4 – 152.7

°C; ^{1}H NMR (400 MHz, $CDCl_3$) δ 9.66 (s, 1H), 8.26 – 8.11 (m, 2H), 7.87 – 7.68 (m, 2H), 7.34 – 7.09 (m, 5H), 3.47 (dd, *J* = 12.2, 6.6 Hz, 2H), 2.87 (s, 3H), 2.69 (t, *J* = 7.3 Hz, 2H), 1.88 – 1.66 (m, 4H); ^{13}C NMR (100 MHz, $CDCl_3$) δ 182.9, 172.9, 166.3, 161.1, 150.9, 142.2, 134.5, 134.0, 132.8, 131.5, 128.4, 128.2, 127.6, 126.7, 126.0, 125.7, 115.5, 39.2, 35.5, 28.9, 28.8, 14.9; HRMS (ESI^+, TOF) calcd for $C_{24}H_{21}NO_4Na$ $[M + Na]^+$ 410.1368, found 410.1374. Sample for biology test was purified by preparative HPLC with HPLC purity >99%.

_N_-(3-(1_H_-imidazol-1-yl) propyl)-2-methylbenzofuran-3-carboxamide (11)

To a stirred solution of 2-methylbenzofuran-3-carboxylic acid (25 mg, 0.14 mmol), DMAP (25.7 mg, 0.21 mmol) and HBTU (80 mg, 0.21 mmol) in DMF (0.7 mL) was added 1-(3-Aminopropyl) imidazole (19 μL, 0.16 mmol) at 0 °C. The solvent was removed by *vacuo* after the reaction mixture was stirred at room temperature for 1 day. The residue was purified by flash column chromatography ($MeOH/CH_2Cl_2$, 0/100 to 1/9) to give **11** as a colorless oil (37 mg, 95 % yield). Rf (5 % $MeOH/CH_2Cl_2$) 0.29; ^{1}H NMR (400 MHz, $CDCl_3$) δ 7.58 – 7.48 (m, 2H), 7.48 – 7.41 (m, 1H), 7.32 – 7.25 (m, 2H), 7.05 (s, 1H), 6.97 (s, 1H), 5.97 (s, 1H), 4.07 (t, *J* = 7.0 Hz, 2H), 3.51 (dd, *J* = 13.1, 6.7 Hz, 2H), 2.71 (s, 3H), 2.15 (quint, *J* = 6.9 Hz, 2H); HRMS (ESI^+, TOF) calcd for $C_{16}H_{18}N_3O_2$ $[M + H]^+$ 284.1399, found 284.1392. Sample for biology test was purified by preparative HPLC with HPLC purity >99%.

7-Fluoro-2-hydroxynaphthalene-1,4-dione (13)

To a solution of KO^{t}Bu (547 mg, 4.873 mmol) in anhydrous *t*-BuOH (7.6 mL) which had previously been saturated with O_2 (bubbled for 10 min) was added a solution of 7-fluoro-1-tetralone **12** (100 mg, 0.609 mmol) in anhydrous *t*-BuOH (2.4 mL), and the resulting red reaction

mixture was stirred at ambient temperature for 30 min under O_2 atmosphere. Then, the reaction mixture was cooled down to 0 °C and acidified with 3M HCl until the pH of the mixture became 1−2. The volatiles were removed in vacuo, and the crude material was extracted with CH_2Cl_2. Combined organic layers were dried over anhydrous sodium sulfate then filtered and concentrated under vacuo to afford 7-fluoro-2-hydroxynaphthalene-1,4-dione **13** as a yellow solid (108 mg, 92 % yield). R_f (EtOAc) 0.38; mp 131.6 – 167.6 °C (decomposed); IR (neat) 3070, 1685, 1650, 1598, 1384, 1349, 1312, 1205, 897, 888, 876, 844, 772 cm^{-1}; ^1H NMR (600 MHz, $CDCl_3$) δ 8.16 (dd, *J* = 8.5, 5.2 Hz, 1H), 7.77 (dd, *J* = 8.1, 2.5 Hz, 1H), 7.46 (td, *J* = 8.4, 2.6 Hz, 1H), 7.27 (brs, 1H), 6.37 (s, 1H); ^{13}C NMR (150 MHz, $CDCl_3$) δ 183.8, 181.2, 166.4, 164.7, 156.4, 131.8, 131.7, 129.8, 129.8, 129.4, 122.3, 122.1, 113.4, 113.2, 110.9; ^{19}F NMR (565 MHz, $CDCl_3$) δ -104.04; HRMS (EI^+, TOF) calcd for $C_{10}H_5FO_3$ $[M]^+$ 192.0223, found 192.0221.

3-(2-Ethoxy-2-oxo-1-(tributylphosphonio)ethyl)-7-fluoro-1,4-dioxo-1,4-dihydronaphthalen-2-olate (14)

To compound **13** (138 mg, 0.718 mmol) with THF (1.0 ml) in a dry and nitrogen-flushed sealed tube at 0 °C was sequentially added ethyl glyoxalate (50% solution in toluene) (263 µL, 1.8 equiv), trifluoroacetic acid (96 µL, 1.8 equiv) and Bu_3P (210 µL, 1.2 equiv), then the reaction mixture was stirred for 3.5 h at 60-64 °C. Solvent was removed under *vacuo* to obtain the crude, which then purified by flash chromatography in neutral Al_2O_3 (EtOAc/*n*-Hexane, 1/1) to provide compound **14** as red gummy liquid (190.0 mg, 63% yield). Rf (1 % MeOH/CH_2Cl_2, neutral Al_2O_3) 0.52; IR (neat) 2960, 2933, 2873, 1718, 1686, 1595, 1377, 1266, 1228 cm^{-1}; ^1H NMR (400 MHz, $CDCl_3$) δ 8.05 – 7.98 (m, 1H), 7.65 (dd, *J* = 6.6, 2.0 Hz, 1H), 7.26 (dd, *J* = 11.2, 5.4 Hz, 1H), 5.31 (dd, *J* = 15.6, 1.1 Hz, 1H), 4.17 – 4.09 (m, 2H), 2.40 – 2.21 (m, 3H), 2.21 – 2.03 (m, 3H), 1.61 –

1.32 (m, 12H), 1.13 (td, J = 7.0, 1.3 Hz, 3H), 0.91 – 0.83 (m, 9H); ^{13}C NMR (100 MHz, $CDCl_3$) δ 183.4, 178.5, 172.0, 169.4, 165.7, 163.1, 134.0, 133.9, 131.3, 128.2, 128.1, 120.2, 120.0, 112.9, 112.6, 105.6, 105.5, 62.2, 37.2, 36.7, 24.1, 24.1, 24.0, 23.9, 20.0, 19.6, 13.8, 13.2; ^{19}F NMR (376 MHz, $CDCl_3$) δ -108.70; HRMS (MALDI$^+$, TOF) calcd for $C_{26}H_{36}FO_5P$ $[M + H]^+$ 479.2362, found 479.2376.

Ethyl-7-fluoro-2-methyl-4,9-dioxo-4,9-dihydronaphtho[2,3-b]furan-3-carboxylate (15)

To compound **14** (393 mg, 0.821 mmol) with THF (4.1 ml) in a dry and nitrogen-flushed round bottom flask at 0 °C was slowly added acetyl chloride (76 µL, 1.3 equiv) and Et_3N (171 µL, 1.5 equiv), then stirred for 15 min. Solvent was removed under *vacuo* to obtain the crude, which then purified by flash chromatography (EtOAc/*n*-Hexane, 1/9) to provide compound **15** as pale yellow solid (199.0 mg, 61% yield). R_f (20 % EtOAc/Hexanes) 0.53; mp 156.5 – 160.2 °C; IR (neat) 2986, 2937, 1716, 1688, 1597, 1542, 1264, 1234, 1157, 1115 cm^{-1}; ^{1}H NMR (600 MHz, $CDCl_3$) δ 8.25 – 8.11 (m, 1H), 7.86 – 7.69 (m, 1H), 7.38 (t, J = 8.0 Hz, 1H), 4.46 – 4.35 (q, J = 7.2 Hz, 2H), 2.70 (s, 3H), 1.43 (t, J = 7.2 Hz, 3H); ^{13}C NMR (150 MHz, $CDCl_3$) δ 177.4, 172.2, 166.9, 165.2, 164.8, 161.8, 151.2, 134.2, 134.2, 130.5, 130.4, 130.1, 128.4, 121.0, 120.8, 113.9, 113.5, 113.4, 61.6, 14.2; ^{19}F NMR (565 MHz, $CDCl_3$) δ -103.31; HRMS (EI$^+$, TOF) calcd for $C_{16}H_{11}FO_5$ $[M]^+$ 302.0591, found 302.0594.

7-Fluoro-2-methyl-4,9-dioxo-4,9-dihydronaphtho[2,3-b]furan-3-carboxylic acid (16)

To compound **15** (355 mg, 1.175 mmol) with THF (9.4 mL) and H_2O (2.35 mL) in a round bottom flask at 0 °C was added 3M $NaOH_{(aq)}$ (1.17 ml, 4.5 eq), then allowed to room temperature for a period of 5 hr. Solvent was removed under *vacuo* then dilute with H_2O and washed with

CH_2Cl_2. The aqueous layer was added 3M $HCl_{(aq)}$ until pH = 1~2, then extracted with EA and Brine. Combined organic layers were dried over anhydrous sodium sulfate then filtered and concentrated under *vacuo* to afford the crude carboxylic acid **16** (313 mg, 97% yield). R_f (10 % MeOH/CH_2Cl_2) 0.38; mp 254.5 – 260.0 °C (decomposed); IR (neat) 3447, 2978, 1684, 1647, 1586, 1550, 1354, 1236 cm^{-1}; ^1H NMR (600 MHz, $CDCl_3$) δ 12.87 (s, 1H), 8.45 – 8.23 (m, 1H), 7.91 (d, *J* = 6.9 Hz, 1H), 7.48 (s, 1H), 2.90 (s, 3H); ^{19}F NMR (565 MHz, $CDCl_3$) δ -98.39; HRMS (EI^+, TOF) calcd for $C_{14}H_7FO_5$ $[M]^+$ 274.0278, found 274.0280.

N-(3-(1H-imidazol-1-yl)propyl)-7-fluoro-2-methyl-4,9-dioxo-4,9-dihydronaphtho[2,3-b]furan-3-carboxamide (RJ-LC-07-48)

To a solution of carboxylic acid **16** (282 mg, 1.028 mmol) with DMF (10.3 mL) in a round bottom flask at room temperature was added DMAP (126 mg, 1.028 mmol), HBTU (468 mg, 1.234 mmol) ,3-(1H-imidazol-1-yl)propan-1-amine (184 µL, 1.542 mmol), then stirred for 6 h. Solvent was removed under *vacuo* to obtain the crude material, which then purified by flash chromatography (MeOH/CH_2Cl_2, 1/9) to provide product **RJ-LC-07-48** (251 mg, 64% yield). Rf (10 % MeOH/CH_2Cl_2) 0.30; mp 153.8 – 171.2 °C (decomposed); IR (neat) 3289, 3101, 1680, 1581, 1266, 1226, 740 cm^{-1}; ^1H NMR (600 MHz, $CDCl_3$) δ 9.74 (s, 1H), 8.27 (dd, *J* = 8.6, 5.1 Hz, 1H), 7.87 (dd, *J* = 8.2, 2.4 Hz, 1H), 7.60 (s, 1H), 7.45 (td, *J* = 8.3, 2.4 Hz, 1H), 7.08 (s, 1H), 7.01 (s, 1H), 4.12 (t, *J* = 7.0 Hz, 2H), 3.47 (t, *J* = 6.0 Hz, 2H), 2.89 (s, 3H), 2.17 (m, 2H); ^{13}C NMR (150 MHz, $CDCl_3$) δ 182.1, 171.7, 167.6, 167.1, 165.9, 161.4, 151.1, 137.3, 134.5, 134.4, 131.0, 131.0, 129.8, 129.2, 126.2, 121.2, 121.1, 118.8, 115.4, 114.2, 114.1, 44.5, 36.3, 30.9, 15.1; ^{19}F NMR (565 MHz, $CDCl_3$) δ -100.63; HRMS ($MALDI^+$, TOF) calcd for $C_{20}H_{16}FN_3O_4$ $[M + H]^+$ 382.1203,

found 382.1201. Sample for biology test was purified by preparative HPLC with HPLC purity >99%.

SCHEME 3. Conjugation of AS4583 analogue onto magnetic beads

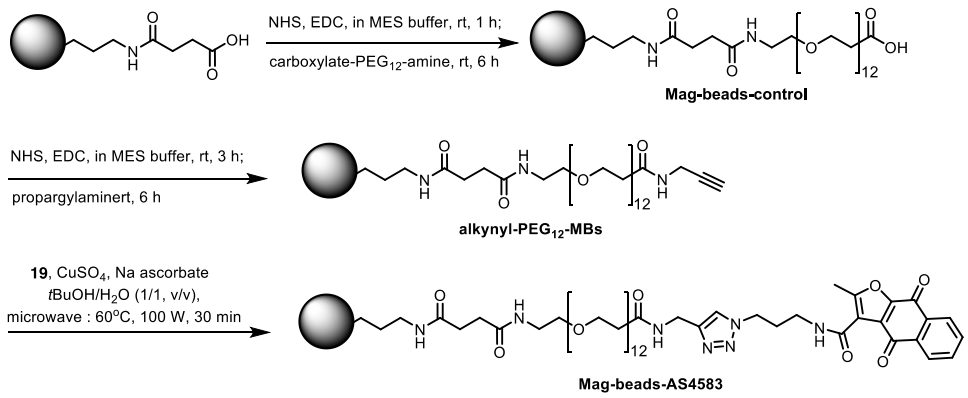

***N*-(3-Azidopropyl)-2-methyl-4, 9-dioxo-4, 9-dihydronaphtho [2, 3-*b*] furan-3-carboxamide (19)**

To a stirred solution of **18** (30.7 mg, 0.12 mmol), HBTU (54.6 mg, 0.144 mmol) and DMAP (14.7 mg, 0.12 mmol) in DMF (0.6 mL) was added 3-azido-1-propylamine (30 μL, 0.3 mmol) at room temperature. The solvent was removed by *vacuo* after the reaction mixture was stirred at room temperature for 3 days. Then the crude was washed by H_2O, extracted with CH_2Cl_2 (10 mL x 3), dried over Na_2SO_4, and concentrated in *vacuo*. The residue was purified by flash column chromatography (MeOH/CH_2Cl_2, 0/100 to 1/49) to give **19** as a yellow solid (18 mg, 43 % yield). R_f (CH_2Cl_2) 0.52; Mp 105.5 – 109.3 °C; IR (neat) 3275, 3084, 2925, 2853, 2099, 1660, 1644, 1580, 1537, 1376, 1260, 1212, 1143, 991, 717 cm^{-1}; ^1H NMR (400 MHz, $CDCl_3$) δ 9.75 (t, J = 4.8 Hz, 1H), 8.24 – 8.18 (m, 2H), 7.82 – 7.75 (m, 2H), 3.55 (dd, J = 12.4, 6.6 Hz, 2H), 3.46 (t, J = 6.8 Hz, 2H), 2.87 (s, 3H), 1.96 (quint, J = 6.7 Hz, 2H); ^{13}C NMR (100 MHz, $CDCl_3$) δ 183.1, 172.9, 166.5,

161.4, 151.0, 134.7, 134.2, 132.8, 131.5, 127.7, 126.8, 126.0, 115.2, 49.2, 36.6, 28.7, 14.9; HRMS (ESI^+, TOF) calcd for $C_{17}H_{14}N_4Na$ $[M + Na]^+$ 361.0913, found 361.0917.

Mag-beads-control

Carboxylate magnetic beads (10 mg) were dispersed into MES (50 mM, pH 6.0, 300 μL). *N*-hydroxysuccinimide (NHS, 3.5 mg, 0.03 mmol) and 1-ethyl-3-(3-dimethylaminopropyl) carbodiimide hydrochloride (EDC-HCl, 5.7 mg, 0.03 mmol) were added to the solution and stirred for 1 hr at room temperature. The resulting beads were washed with PBS (50 mM, pH 7.0, 300 μL x 2) to remove excess NHS and EDC-HCl. 200 μL of 1 mM carboxylated-PEG_{12}-amine (pH 7.8 in 50 mM HEPES) was added to the beads and then stirred for 6 hr at room temperature. After separation with a magnet, the beads were washed with MES (50 mM, pH 6.0) to give **carboxyl-PEG_{12}-MBs**.

Alkynyl-PEG_{12}-MBs

Carboxyl-PEG_{12}-MBs (10 mg) were dispersed into MES (50 mM, pH 6.0, 300 μL). *N*-hydroxysuccinimide (NHS, 3.5 mg, 0.03 mmol) and 1-ethyl-3-(3-dimethylaminopropyl) carbodiimide hydrochloride (EDC-HCl, 5.7 mg, 0.03 mmol) were added to the solution and stirred for 3 hr at room temperature. The resulting beads were washed with PBS (50 mM, pH 7.0, 300 μL x 2) to remove excess NHS and EDC-HCl. 200 μL of 1 mM propargylamine (pH 7.0 in 50 mM PBS) was added to the beads and then stirred for 6 hr at room temperature. After separation with a magnet, the beads were washed with MES (50 mM, pH 6.0) to give **alkynyl-PEG_{12}-MBs**.

Mag-beads-AS4583

To a solution of alkynyl-PEG_{12}-MBs (10 mg), azide **19** (1.3 mg, 4.0 μmol), $CuSO_4$ in 0.1 M H_2O (5 μL, 0.5 μmol) and sodium ascorbate in 0.1 M H_2O (2 μL, 0.2 μmol) was in *t*-Butanol/H_2O (0.2 mL, 1/1, v/v) and in Microwave condition: 100 W, 60 ºC for 30 min. After separation with a magnet, the beads were washed with MES (50 mM, pH 6.0) to give **Mag-beads-AS4583**.

High-throughput screening (HTS)

HTS was performed against a collection of the 2 M compound library. The synthetic molecules in the 2 M library were clustered into approximately 5,300 groups based on 85% structure similarity. The diversity was approximately 0.87, as calculated by a modified centroid-diversity sorting algorithm. Screens were performed in 1,536-well plates using the HTS system manufactured by GNF systems (San Diego, CA). For primary screening, H1975 cells were dispensed into the wells of a 1,536-well plate at 400 cells/well. The cells were incubated for 3 days in environmentally controlled incubators (37 °C, 5% CO_2, 80% humidity), and cell viability was monitored using Cell- TiterGlo (Promega). The compounds resulting in a >80% decrease in luminescence were selected using a hit-picking system (GNF System, San Diego, CA) and collected in 1,536-well plates. Serial dilutions of hit plates were performed with an automatic liquid handling system (Bravo™, Agilent) and used for downstream screening with other lung cancer cells. IC_{50} values were calculated using a proprietary software program (GNF Systems, San Diego).

Cell lines and culture conditions

The human lung adenocarcinoma cell lines CL1-0 and CL1-5 were established in our laboratory as previously described[29]. The human lung cancer cell line NCI-H1975, A549 (a human

lung adenocarcinoma epithelial cell line), as well as the BEAS-2B and Hs68 cell lines, were purchased from the American Type Culture Collection (Manassas, VA). The cell line PC9 and derivative PC9/IR clones were kind gifts from Dr. C. H. Yang (Graduate Institute of Oncology, Cancer Research Center, and National Taiwan University). NBE cultured in BEBM (bronchial epithelial basal media) was kindly provided by Dr. Reen Wu (Department of Anatomy, Physiology and Cell Biology, University of California Davis). Cells were grown in RPMI or DMEM medium containing 10% FBS and 2 mM L-glutamine (all from Invitrogen, Eugene, OR) at 37 °C in a humidified atmosphere of 5% CO_2-95% air.

Sulforhodamine B colorimetric assay for cytotoxicity screening

Prior to the experiment, 2×10^3 cells were cultured in 96-well plates for 24 h. The culture medium was replaced with fresh medium containing the appropriate concentration of compound ranging from 0.005 μM to 10 μM for 72 h. After an incubation period, the cells were fixed with 10% trichloroacetic acid and stained with 0.4% (w/v) sulforhodamine B dissolved in 1% acetic acid for 30 min. Then, the excess dye was removed by washing the samples repeatedly with 1% acetic acid. The protein-bound dye was dissolved in 10 mM Tris-base solution for the determination of optical density at 510 nm using a microplate reader. The cell growth curve was plotted using GraphPad software (San Diego, CA).

MTS assay

For MTS assay, fresh prepare 20 μl of MTS stock solution mix with 100 μl culture media to each well. After more than one hour of incubation, absorption was measured at 490 nm by a spectrophotometer (Molecular Devices).

Xenograft tumor growth *in vivo*

The in vivo Xenograft tumor growth assay was performed as described previously[18]. Briefly, male BALB/c-nu mice (5 weeks of age) were obtained from National Laboratory Animal Center, Taiwan, and acclimatized to laboratory conditions for 1 week before tumor implantation. A total of $3x10^6$ H1975 cells were subcutaneously injected into the flank of the BALB/c-nu mice; and the drug treatment was initiated at 4 days after the inoculation of cancer cells. The control group was five days a week treated intraperitoneally with DMSO in 50% PEG400, whereas the compound group was treated with 1 mg/kg or 4 mg/kg in 50% PEG400 for 4 weeks (n=10 per group). During the treatment, tumor size and body weights were measured every 3 to 4 days.; and the tumor size was calculated as $V = 1/2\times (\text{length}) \times (\text{width})^2$. Tumor growth curves are presented as mean ± standard error of the mean (SEM). % Tumor Growth Inhibition (TGI) was calculated as follows: $[1 - ((T_{final} - T_{initial})/ (C_{final} - C_{initial}))] *100$, where T = AS4583-treated tumor volumes and C = control-treated tumor volumes at treatment start and after 27 days' treatment. All mouse experiments were performed in accordance with the animal guidelines and with the approval of the Laboratory Animal Center, National Taiwan University College of Medicine (IACUC No: 20150378).

Cell-cycle analysis

H1975 cells were seeded at a density of 5×10^4 in 60-mm culture dishes for 24 h before the experiment. The cells were treated with 0–140 nM of compound for 72 h in complete medium. The cells were harvested with 0.1% trypsin solution containing 0.05% EDTA in PBS, centrifuged,

washed with PBS, and re-suspended in cold 70% ethanol. The cells were then stained with propidium iodide (50 μg/ml; Sigma) for 30 min and subjected to flow cytometric analysis with a FACStar Plus (Becton Dickinson, San Francisco, CA).

BrdU incorporation

For BrdU (5'-Bromo-2'-deoxyuridine) labeling, the cells were pre-cultured for 24 h, treated for 0, 3, 6, 12, 24, or 48 h and pulse-labeled for 30 min with 10 μM BrdU (BioVision, Inc., Milpitas, CA). Cells were fixed and permeabilized with Cytofix/Cytoperm Buffer (BD Pharmingen™ BrdU Flow Kit Staining, BD Bioscience, San Jose, CA) and treated with DNase to expose incorporated BrdU. The BrdU content was assessed using fluorescent antibodies. DNA was stained with 7-Aminoactinomycin D (7-AAD). The samples were analyzed in a FACS caliber flow cytometer (Becton Dickinson, Sweden) for dot plot histogram analysis (BrdU incorporation vs. DNA content).

Cell synchronization and immunofluorescence

H1975 cells were arrested in G1 by contact inhibition. After 3 d, the cells were re-plated at a low density on cover slips and allowed to progress through the cell cycle. The cells were pulsed with 140 nM of compound for 48 h and were fixed for 10 min at room temperature in 3.7% cold paraformaldehyde in PBS (pH 7.2), washed 3 times with PBS, and permeabilized for 10 min at room temperature in PBS containing 0.1% Triton X-100. The cells were blocked with PBS containing 3% bovine serum albumin and stained overnight at 4°C with primary antibodies against MCM2, followed by incubation for 1 h at 37°C with Alexa Fluor 488 Goat Anti-Mouse IgG (Life Technologies Corporation). The cells were mounted onto microscope slides with ProLong Gold

Antifade Reagent with DAPI (Life Technologies Corporation) and then examined and photographed using a Zeiss LSM 700 Confocal microscope (Zeiss, Urbana, IL).

Lentiviral shRNA induction

The lentiviruses used in this study were generated by co-transfection of HEK293T cells with the lentiviral vector pLKO.1-shMCM2 from the National RNAi Core Facility (Academia Sinica, Taiwan) and two helper plasmids (pCMV△R8.91, pMD.G) using Lipofectamine 2000. The virus-containing medium was collected at 24, 48, and 72 h post-transfection, centrifuged, and filtered through a 0.45-mm pore-size filter. The cells were infected with the various individual lentiviruses in medium containing polybrene (8 μg/ml). At 24 h post-infection, the cells were incubated in fresh medium for 48 h and used for other experiments.

Plasmids and antibodies

Briefly, the MCM2 full-length DNA fragments were amplified via RT-PCR from H1975 cDNA and sub-cloned into pJET1.2 (Thermo) to generate pJET-MCM2. The MCM2 DNA fragment was inserted between the NheI and EcoRI sites of p3xFlag to generate p3xFlag-MCM2. Expression vectors for myc-tagged ubiquitin have been described[30]. The primary antibodies specific for Myc, ubiquitin, cyclins E, A, B, and D1, and MCM2, 3, 4, 5, 6 and 7 were purchased from Santa Cruz Biotechnology (Santa Cruz, CA).

Transfection

Briefly, cells were seeded in 10-cm plates at a density of 3×10^5 cells/ml in RPMI medium with 10% fetal bovine serum for 24 h. The 70% confluent cells were transfected with plasmids (5

μg each) using 20 U Lipofectamine 2000 reagent (Invitrogen) in a total volume of 1 ml of Opti-MEM (all from Invitrogen). At 36 h post-transfection, the cells were incubated in the absence or presence of each compound (140 nM) and MG132 (10 μM; Sigma, St. Louis, MO). After 12 h, the cells were harvested for further analysis.

Immunoprecipitation and immunoblotting

Briefly, H1975 cells were plated and cultured in complete RPMI medium and allowed to attach for 24 h, followed by the addition of 140 nM of a compound. The incubation was continued for 24, 48, or 72 h. Control cells were maintained in regular medium. The cells were lysed on ice for 30 min in ice-cold immunoprecipitation buffer containing 20 mM Tris (pH 8.0), 150 mM NaCl, 100 μM Na_3VO_4, 50 mM NaF, 30 mM sodium pyrophosphate, 0.5% (v/v) NP-40 (Sigma) and a 25-fold dilution of a stock solution treated with one mini-protease inhibitor cocktail tablet (Roche Diagnostics, Basel, Switzerland) dissolved in 2 ml distilled water. The cell lysates were passed several times through a 21-gauge needle and clarified by centrifugation at 8,000 × *g* for 30 min at 4°C. The supernatants were collected, and the protein content of each lysate was determined with the BCA Protein Assay Reagent (Pierce, Rockford, IL, USA) using bovine serum albumin as the standard. Aliquots of the lysates were incubated in immunoprecipitation buffer with respective antibodies overnight at 4°C. Dynabeads Protein A/G (Invitrogen) was added and incubated for 1 h, then washed six times with PBS (phosphate-buffered saline; 0.01 M sodium phosphate, 0.14 M NaCl, pH 7.4; Sigma). For immunoblotting, the proteins were resolved using SDS-PAGE (8% or 10% acrylamide). The proteins were transferred to a polyvinylidene difluoride membrane and blocked in TBST buffer (10 mM Tris, pH 7.5, 100 mM NaCl and 0.05% (v/v) Tween 20) containing 3% nonfat dried milk. The blots were incubated with various primary antibodies and

incubated for 1 h with appropriate secondary antibodies conjugated to horseradish peroxidase in TBST. The intensity of each specific immunoreactive band was detected by enhanced chemiluminescence according to the manufacturer's protocol (PerkinElmer, Inc., USA), quantified by densitometry, and normalized against the loading control (β-actin) with Image J software.

Chromatin loading assay

After washing with cold PBS, H1975 cells were harvested using 0.1% trypsin, and cell pellets were lysed by incubating the pellets in cytoskeleton buffer (20 mM HEPES, pH 7.4, 100 mM NaCl, 3 mM $MgCl_2$, 300 mM sucrose, and 0.1% (v/v) NP-40) for 15 min on ice. Detergent-soluble fractions were obtained after low-speed centrifugation (3,000 × *g*) at 4°C. The pellets were rinsed with cytoskeleton buffer for 10 min on ice and re-centrifuged to obtain a chromatin-enriched fraction. The pellets were then sonicated for 5 s in cytoskeleton buffer for 30 min and subjected to high-speed centrifugation (16,000 × *g*). The post-sonication supernatant was designated as the chromatin-bound fraction.

Site-directed mutagenesis

Briefly, p3xFlag-MCM2 plasmids were used as templates for PCR-based site-directed mutagenesis with the QuikChange Lightning site-directed mutagenesis kit (Stratagene). The primers used to generate p3xFlag-MCM2-Q341A (mutated nucleotides are underlined) were 5'-CTG GGT CCT TTC TGC GCG TCC CAG AAC CAG G-3' (forward) and 5'-CCT GGT TCT GGG ACGCGC AGA AAG GAC CCA G-3' (reverse).

Homology modeling, MD and ligand docking

We used the Phyre2 server[31] to search the initial template for modeling and to calculate the target–template sequence alignment. The structure of human MCM2 (residues 192 to 804) was modeled using MODELLER 9v12[32]. To improve the model quality, the model with the best discrete optimized protein energy (DOPE) score was subjected to molecular dynamics simulation using GROMACS version 4.6.2[33] with an OPLS-AA force field as a preparatory process for docking. The initial structure was immersed in an orthorhombic water box, and the net charge was neutralized by adding sodium or chloride ions (at 150 mM salt concentration). Long-range electrostatics were handled using the particle mesh Ewald method. The steepest descent energy minimization was used to remove possible bad contacts from the initial structures until energy convergence reached 1,000 kJ/ (mol·nm). The systems were subjected to equilibration at 300 K and a normal pressure constant (1 bar) for 100 ps under the conditions of position restraints for heavy atoms and LINCS constraints. The equilibrated structures were used to perform the production run. The time step of the simulation was set to 2 fs, and the coordinates were saved for analysis every 100 ps. ProSA[34] and PROCHECK[35] were used to validate the stereochemical qualities of the final model.

The coordinates of compound AS4583 were obtained from the PubChem database[31] through the unique chemical structure identifier CID: 3585487. The potential AS4583 binding pocket was predicted using iGEMDOCK[36]. AutoDock Vina version 1.1.2[37] was used to construct the MCM2-ligand complex structure. We centered the grid box (30 × 30 × 30 Å) at the putative ligand-binding pocket. Because each docking run produces 20 binding modes, to increase the chance of finding the best binding mode, we repeated each docking run 10 times using an exhaustiveness value of 64 and ranked the resulting 200 poses based on their predicted binding

affinity (in kcal/mol). The top ranked results were visualized and analyzed with PyMOL[38] and the AutoDock plugin[39].

For the MCM2-7 hexamer structure, each protomer was roughly built using the Phyre2 server and then assembled into a hexamer by applying the 6-fold symmetry from the crystal structure of *Methanothermobacter* MCM (PDB ID1 LTL)[25]. The clashes between neighboring protomers were gradually removed using the loop optimization protocol in MODELLER[32].

Statistical analysis

The data are shown as the mean ± SEM. Statistical analyses were performed by Student's t-test or Pearson's x^2 test. The overall survival rates for patient groups with different expression signatures were determined using SPSS software (v10.0; SPSS, Inc., Chicago, IL) to apply the Kaplan–Meier method and two-sided log-rank tests. *P* values of 0.05 were considered statistically significant.

ASSOCIATED CONTENT

Supporting Information

The Supporting Information is available free of charge on the ACS Publications website at DOI:

Molecular formula strings (csv)

NMR spectra (pdf)

Supplementary data (pdf)

AUTHOR INFORMATION

Corresponding Author

*Correspondence to: Dr. Szu-Hua Pan (e-mail: shpan@ntu.edu.tw, Phone: +886-2-23123456 ext. 88661; Fax: +886-2-33936523, Address: 5F, No.2, Xuzhou Rd., Zhongzheng Dist., Taipei City 100, Taiwan) and Dr. Rong-Jie Chein (e-mail: rjchein@chem.sinica.edu.tw, Phone: +886-2-27898526; Fax: +886-27831237, Address: 128 Academia Road Sec. 2, Nankang Taipei 115 Taiwan)

Funding Sources

The authors thank National Taiwan University (NTU-CDP- 104R7879, 105R7879), Academia Sinica (AS-SUMMIT-108), the Ministry of Science and Technology (Taiwan) (NSC 102-2314-B-002-046-MY3, 102-2923-B-002-004, 103-2923-B-002-003, MOST 104-0210-01-09-02, 105-2628-B-002 -007 -MY3, 105-0210-01-13-01, 106-0210-01-15-02, 107-0210-01-19-01, 108-3114-Y-001-002, 108-2314-B-002 -191 -MY3), and the National Research Program for Biopharmaceuticals (ChemBank and High-Throughput Screening Resource Center, NSC-100-2325-B-001-022, 101-2325-B-001-029, and 102-2325-B-001-041) for supporting this study.

Notes

The authors declare no conflict of interest.

ACKNOWLEDGMENT

The authors also thank the following individuals for providing technical support: Dr. Wen-Long Wang (Department of Internal Medicine, National Cheng Kung University, Tainan, Taiwan), Dr. Yih-Leong Chang and Dr. Chen-Tu Wu (Department of Pathology and Graduate Institute of Pathology, College of Medicine, National Taiwan University), Dr. Lee-Jene Teng and Miss Yu-Tzu Lin (Department of Clinical Laboratory Sciences and Medical Biotechnology, College of Medicine, National Taiwan University).

ABBREVIATIONS

NSCLC, non-small-cell lung cancer; HTS, high-throughput screening; MCM, minichromosomal maintenance protein; TKIs, tyrosine kinase inhibitors; EGFR, epithelial growth factor receptor; Cdc6, cell division cycle 6; GINS (Go, Ichi, Nii, andSan; five, one, two, and three in Japanese); ORC, Origin recognition complex; SAR, structure activity relationship; CV, coefficient of variation; WH, winged-helix; MD, molecular dynamics; Chk1, checkpoint kinase 1.

REFERENCES

(1) Siegel, R. L.; Miller, K. D.; Jemal, A. Cancer Statistics, 2019. *CA Cancer J Clin* **2019,** 69, 7-34.

(2) Nguyen, K. S.; Kobayashi, S.; Costa, D. B. Acquired Resistance to Epidermal Growth Factor Receptor Tyrosine Kinase Inhibitors in Non-Small-Cell Lung Cancers Dependent on the Epidermal Growth Factor Receptor Pathway. *Clin Lung Cancer* **2009,** 10, 281-289.

(3) Nguyen, K. S.; Neal, J. W. First-Line Treatment of Egfr-Mutant Non-Small-Cell Lung Cancer: The Role of Erlotinib and Other Tyrosine Kinase Inhibitors. *Biologics* **2012,** 6, 337-345.

(4) Swinney, D. C.; Anthony, J. How Were New Medicines Discovered? *Nat Rev Drug Discov* **2011,** 10, 507-519.

(5) Arteaga, C. L.; Johnson, D. H. Tyrosine Kinase Inhibitors-Zd1839 (Iressa). *Curr Opin Oncol* **2001,** 13, 491-498.

(6) Moyer, J. D.; Barbacci, E. G.; Iwata, K. K.; Arnold, L.; Boman, B.; Cunningham, A.; DiOrio, C.; Doty, J.; Morin, M. J.; Moyer, M. P.; Neveu, M.; Pollack, V. A.; Pustilnik, L. R.; Reynolds, M. M.; Sloan, D.; Theleman, A.; Miller, P. Induction of Apoptosis and Cell Cycle Arrest by Cp-358,774, an Inhibitor of Epidermal Growth Factor Receptor Tyrosine Kinase. *Cancer Res* **1997,** 57, 4838-4848.

(7) Cui, J. J.; Tran-Dube, M.; Shen, H.; Nambu, M.; Kung, P. P.; Pairish, M.; Jia, L.; Meng, J.; Funk, L.; Botrous, I.; McTigue, M.; Grodsky, N.; Ryan, K.; Padrique, E.; Alton, G.; Timofeevski, S.; Yamazaki, S.; Li, Q.; Zou, H.; Christensen, J.; Mroczkowski, B.; Bender, S.; Kania, R. S.; Edwards, M. P. Structure Based Drug Design of Crizotinib (Pf-02341066), a Potent and Selective Dual Inhibitor of Mesenchymal-Epithelial Transition Factor (C-Met) Kinase and Anaplastic Lymphoma Kinase (Alk). *J Med Chem* **2011,** 54, 6342-6363.

(8) Buchdunger, E.; Zimmermann, J.; Mett, H.; Meyer, T.; Muller, M.; Druker, B. J.; Lydon, N. B. Inhibition of the Abl Protein-Tyrosine Kinase in Vitro and in Vivo by a 2-Phenylaminopyrimidine Derivative. *Cancer Res* **1996,** 56, 100-104.

(9) Hartford, C. M.; Ratain, M. J. Rapamycin: Something Old, Something New, Sometimes Borrowed and Now Renewed. *Clin Pharmacol Ther* **2007,** 82, 381-388.

(10) Medina, T.; Amaria, M. N.; Jimeno, A. Dabrafenib in the Treatment of Advanced Melanoma. *Drugs Today (Barc)* **2013,** 49, 377-385.

(11) Moffat, J. G.; Rudolph, J.; Bailey, D. Phenotypic Screening in Cancer Drug Discovery - Past, Present and Future. *Nat Rev Drug Discov* **2014,** 13, 588-602.

(12) Marks, P. A.; Breslow, R. Dimethyl Sulfoxide to Vorinostat: Development of This Histone Deacetylase Inhibitor as an Anticancer Drug. *Nat Biotechnol* **2007,** 25, 84-90.

(13) Nakajima, H.; Kim, Y. B.; Terano, H.; Yoshida, M.; Horinouchi, S. Fr901228, a Potent Antitumor Antibiotic, Is a Novel Histone Deacetylase Inhibitor. *Exp Cell Res* **1998,** 241, 126-133.

(14) O'Dwyer, K.; Maslak, P. Azacitidine and the Beginnings of Therapeutic Epigenetic Modulation. *Expert Opin Pharmacother* **2008,** 9, 1981-1986.

(15) Kotla, V.; Goel, S.; Nischal, S.; Heuck, C.; Vivek, K.; Das, B.; Verma, A. Mechanism of Action of Lenalidomide in Hematological Malignancies. *J Hematol Oncol* **2009,** 2, 36.

(16) Gintant, G. A.; George, C. H. Introduction to Biological Complexity as a Missing Link in Drug Discovery. *Expert Opin Drug Discov* **2018,** 13, 753-763.

(17) Chen, W. J.; Ho, C. C.; Chang, Y. L.; Chen, H. Y.; Lin, C. A.; Ling, T. Y.; Yu, S. L.; Yuan, S. S.; Chen, Y. J.; Lin, C. Y.; Pan, S. H.; Chou, H. Y.; Chen, Y. J.; Chang, G. C.; Chu, W. C.; Lee, Y. M.; Lee, J. Y.; Lee, P. J.; Li, K. C.; Chen, H. W.; Yang, P. C. Cancer-Associated

Fibroblasts Regulate the Plasticity of Lung Cancer Stemness Via Paracrine Signalling. *Nat Commun* **2014,** 5, 3472.

(18) Kuo, T. C.; Li, L. W.; Pan, S. H.; Fang, J. M.; Liu, J. H.; Cheng, T. J.; Wang, C. J.; Hung, P. F.; Chen, H. Y.; Hong, T. M.; Hsu, Y. L.; Wong, C. H.; Yang, P. C. Purine-Type Compounds Induce Microtubule Fragmentation and Lung Cancer Cell Death through Interaction with Katanin. *J Med Chem* **2016,** 59, 8521-8534.

(19) Feng, D.; Tu, Z.; Wu, W.; Liang, C. Inhibiting the Expression of DNA Replication-Initiation Proteins Induces Apoptosis in Human Cancer Cells. *Cancer Res* **2003,** 63, 7356-7364.

(20) Yamauchi, M.; Yamaguchi, R.; Nakata, A.; Kohno, T.; Nagasaki, M.; Shimamura, T.; Imoto, S.; Saito, A.; Ueno, K.; Hatanaka, Y.; Yoshida, R.; Higuchi, T.; Nomura, M.; Beer, D. G.; Yokota, J.; Miyano, S.; Gotoh, N. Epidermal Growth Factor Receptor Tyrosine Kinase Defines Critical Prognostic Genes of Stage I Lung Adenocarcinoma. *PLoS One* **2012,** 7, e43923.

(21) Forsburg, S. L. Eukaryotic Mcm Proteins: Beyond Replication Initiation. *Microbiol Mol Biol Rev* **2004,** 68, 109-131.

(22) Emanuele, M. J.; Elia, A. E.; Xu, Q.; Thoma, C. R.; Izhar, L.; Leng, Y.; Guo, A.; Chen, Y. N.; Rush, J.; Hsu, P. W.; Yen, H. C.; Elledge, S. J. Global Identification of Modular Cullin-Ring Ligase Substrates. *Cell* **2011,** 147, 459-474.

(23) Wu, Z. Z.; Jang, Y. J.; Lee, C. J.; Lee, Y. T.; Lin, W. A Versatile and Practical Method for Regioselective Synthesis of Polysubstituted Furanonaphthoquinones. *Org Biomol Chem* **2013,** 11, 828-834.

(24) Sakakibara, N.; Kelman, L. M.; Kelman, Z. Unwinding the Structure and Function of the Archaeal Mcm Helicase. *Mol Microbiol* **2009,** 72, 286-296.

(25) Fletcher, R. J.; Bishop, B. E.; Leon, R. P.; Sclafani, R. A.; Ogata, C. M.; Chen, X. S. The Structure and Function of Mcm from Archaeal M. Thermoautotrophicum. *Nat Struct Biol* **2003,** 10, 160-167.

(26) Fletcher, R. J.; Chen, X. S. Biochemical Activities of the Bob1 Mutant in Methanobacterium Thermoautotrophicum Mcm. *Biochemistry* **2006,** 45, 462-467.

(27) Chen, S.; Qu, X.; Wan, P.; Li, Q. W.; Wang, Z.; Guo, F.; Bai, L.; Hu, Z.; Tan, W.; Li, J. Norcantharidin Inhibits Pre-Replicative Complexes Assembly of Hepg2 Cells. *Am J Chin Med* **2013,** 41, 665-682.

(28) Liu, Y.; He, G.; Wang, Y.; Guan, X.; Pang, X.; Zhang, B. Mcm-2 Is a Therapeutic Target of Trichostatin a in Colon Cancer Cells. *Toxicol Lett* **2013,** 221, 23-30.

(29) Chu, Y. W.; Yang, P. C.; Yang, S. C.; Shyu, Y. C.; Hendrix, M. J.; Wu, R.; Wu, C. W. Selection of Invasive and Metastatic Subpopulations from a Human Lung Adenocarcinoma Cell Line. *Am J Respir Cell Mol Biol* **1997,** 17, 353-360.

(30) Wang, S. P.; Wang, W. L.; Chang, Y. L.; Wu, C. T.; Chao, Y. C.; Kao, S. H.; Yuan, A.; Lin, C. W.; Yang, S. C.; Chan, W. K.; Li, K. C.; Hong, T. M.; Yang, P. C. P53 Controls Cancer Cell Invasion by Inducing the Mdm2-Mediated Degradation of Slug. *Nat Cell Biol* **2009,** 11, 694-704.

(31) Kelley, L. A.; Sternberg, M. J. Protein Structure Prediction on the Web: A Case Study Using the Phyre Server. *Nat Protoc* **2009,** 4, 363-371.

(32) Eswar, N.; Webb, B.; Marti-Renom, M. A.; Madhusudhan, M. S.; Eramian, D.; Shen, M. Y.; Pieper, U.; Sali, A. Comparative Protein Structure Modeling Using Modeller. *Curr Protoc Protein Sci* **2007,** Chapter 2, Unit 2 9.

(33) Pronk, S.; Pall, S.; Schulz, R.; Larsson, P.; Bjelkmar, P.; Apostolov, R.; Shirts, M. R.; Smith, J. C.; Kasson, P. M.; van der Spoel, D.; Hess, B.; Lindahl, E. Gromacs 4.5: A High-Throughput and Highly Parallel Open Source Molecular Simulation Toolkit. *Bioinformatics* **2013,** 29, 845-854.

(34) Wiederstein, M.; Sippl, M. J. Prosa-Web: Interactive Web Service for the Recognition of Errors in Three-Dimensional Structures of Proteins. *Nucleic Acids Res* **2007,** 35, W407-410.

(35) Laskowski, R. A.; MacArthur, M. W.; Moss, D. S.; Thornton, J. M. Procheck: A Program to Check the Stereochemical Quality of Protein Structures. *J. Appl. Cryst.* **1993,** 26, 283-291.

(36) Wang, Y.; Suzek, T.; Zhang, J.; Wang, J.; He, S.; Cheng, T.; Shoemaker, B. A.; Gindulyte, A.; Bryant, S. H. Pubchem Bioassay: 2014 Update. *Nucleic Acids Res* **2014,** 42, D1075-1082.

(37) Trott, O.; Olson, A. J. Autodock Vina: Improving the Speed and Accuracy of Docking with a New Scoring Function, Efficient Optimization, and Multithreading. *J Comput Chem* **2010,** 31, 455-461.

(38) Hsu, K. C.; Chen, Y. F.; Lin, S. R.; Yang, J. M. Igemdock: A Graphical Environment of Enhancing Gemdock Using Pharmacological Interactions and Post-Screening Analysis. *BMC Bioinformatics* **2011,** 12 Suppl 1, S33.

(39) DeLano, W. L. *The Pymol Molecular Graphics System*, 1.5.0.4; Schrödinger, LLC.: 2004.

Table of Content (Graphic Abstract)

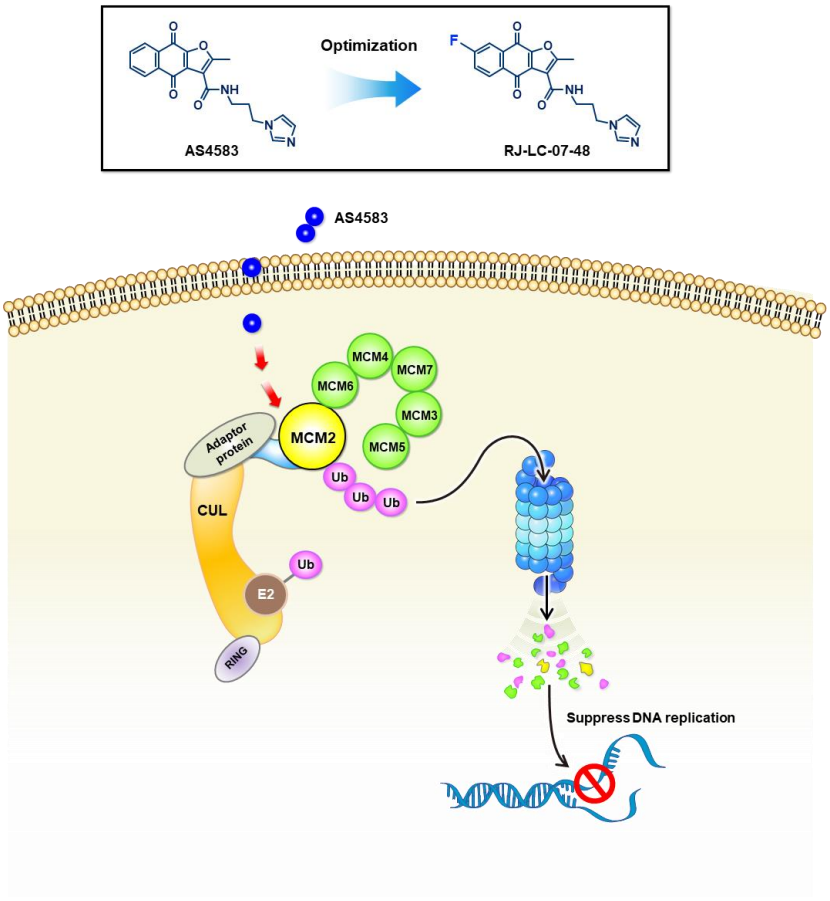

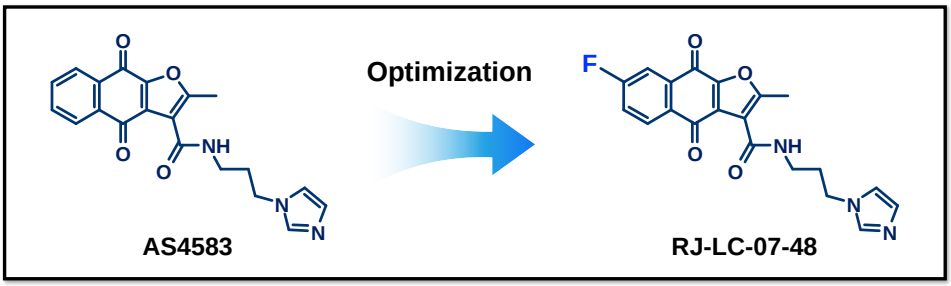
Optimization
F
NH
O
N
AS4583
RJ-LC-07-48

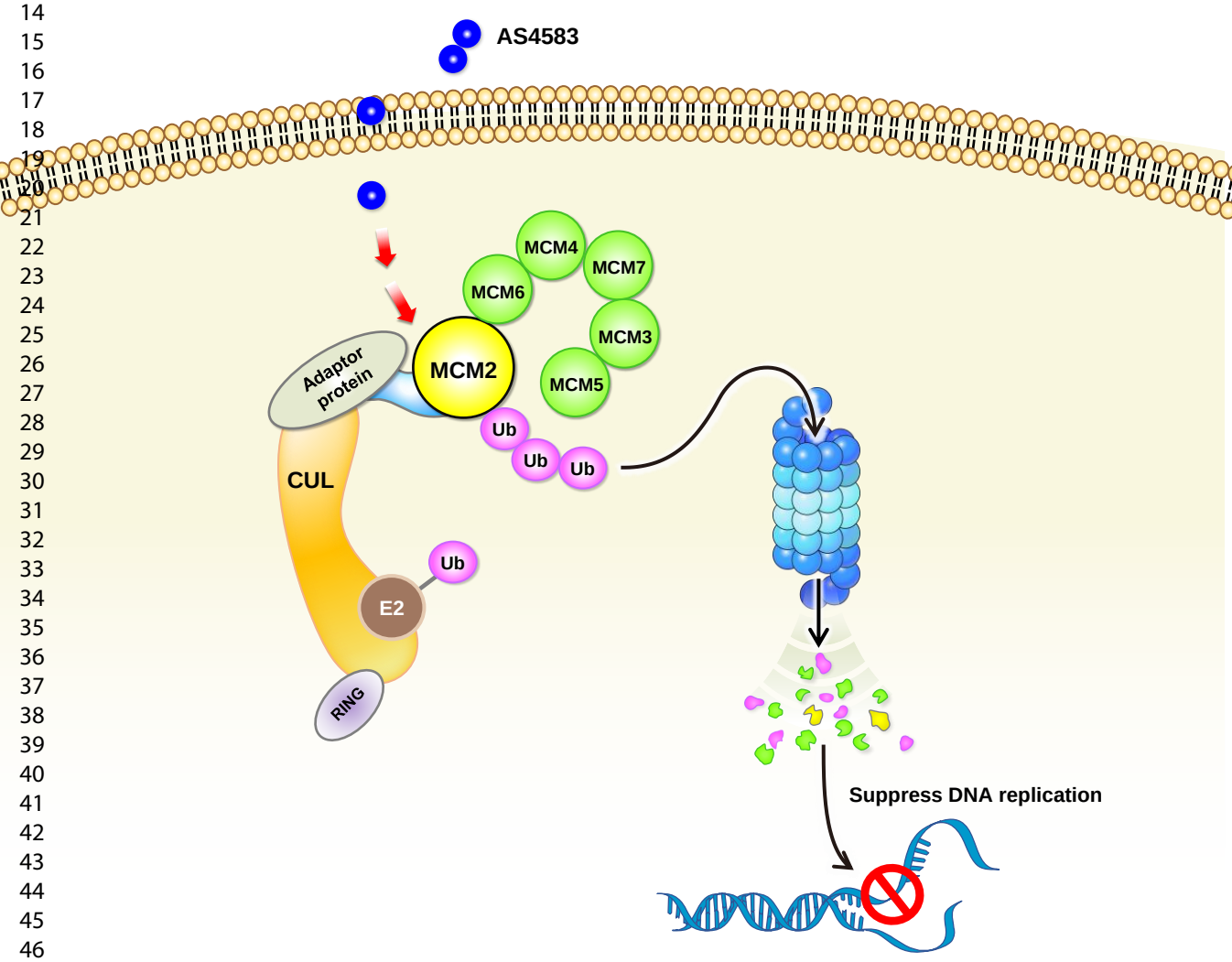
AS4583
MCM4
MCM7
MCM6
MCM3
MCM2
MCM5
Adaptor protein
Ub
Ub
Ub
CUL
Ub
E2
RING
Suppress DNA replication

Lin et. al. Figure 1

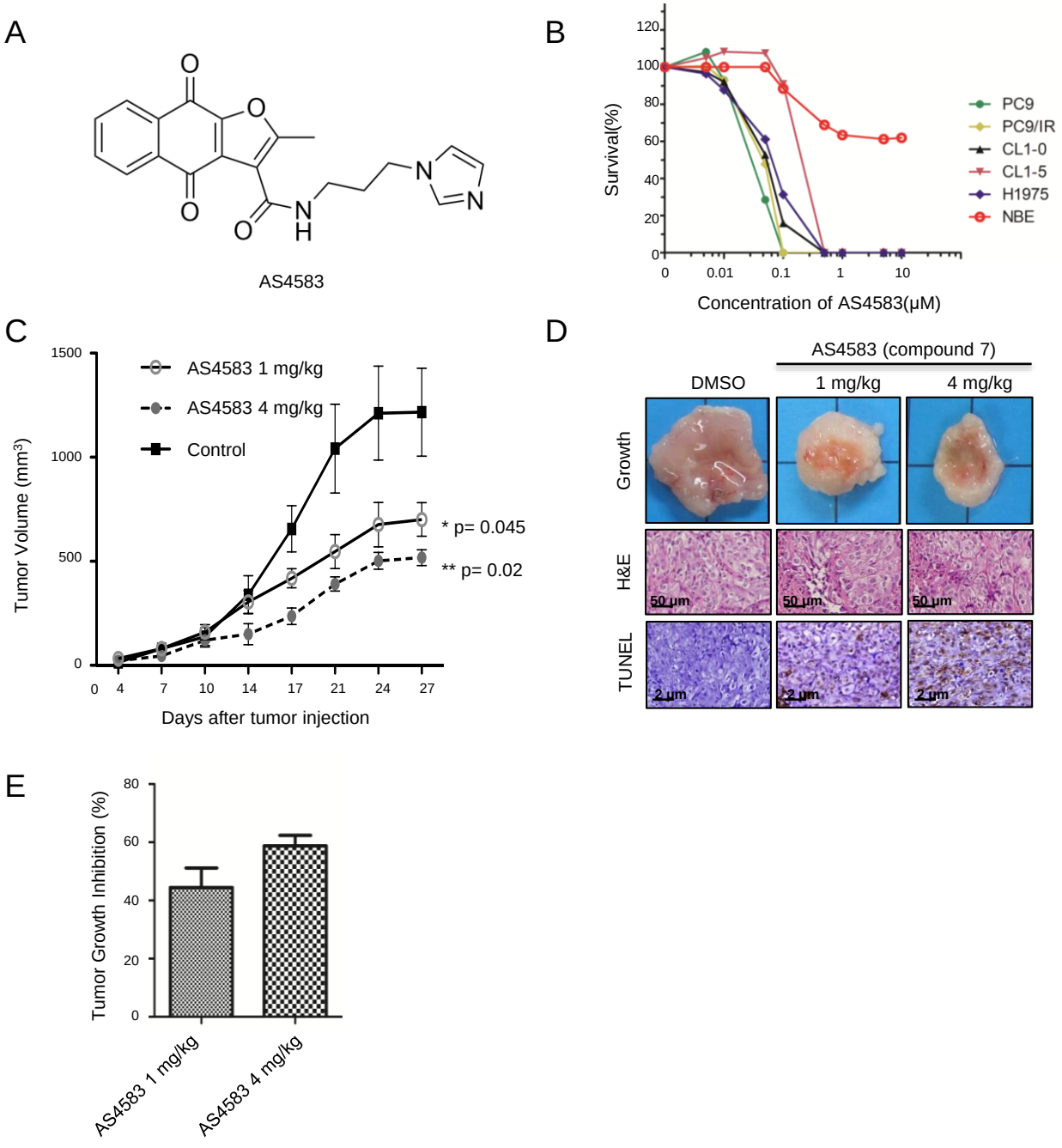

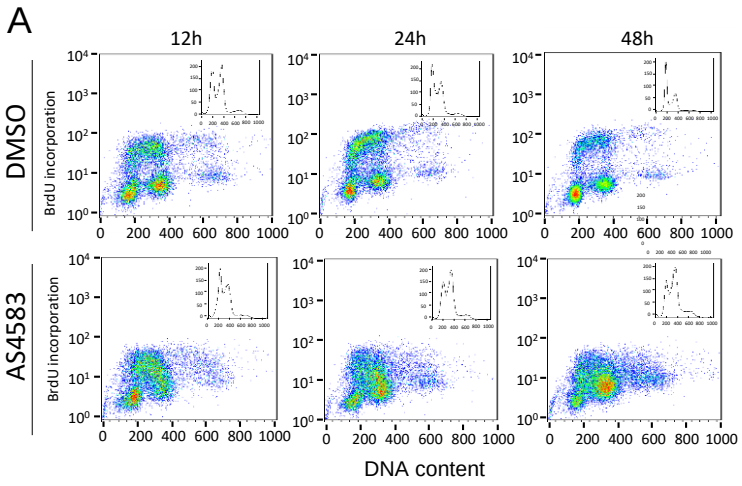
A
12h
24h
48h
DMSO
AS4583
BrdU incorporation
DNA content

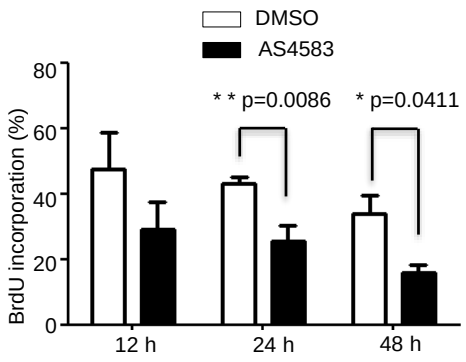
B
DMSO
AS4583
* * p=0.0086
* p=0.0411
BrdU incorporation (%)
12 h
24 h
48 h

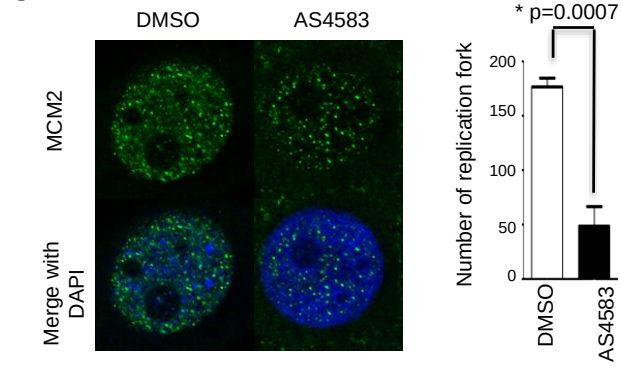
C
DMSO
AS4583
MCM2
Merge with DAPI
* p=0.0007
Number of replication fork
DMSO
AS4583

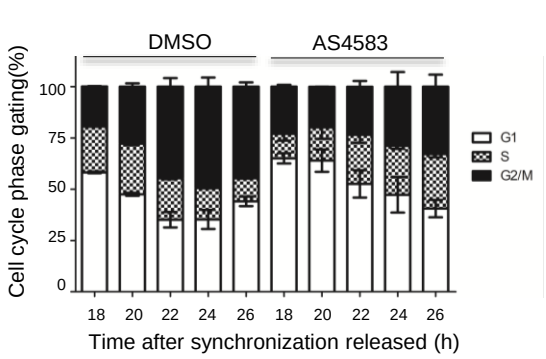
D
DMSO
AS4583
Cell cycle phase gating(%)
G1
S
G2/M
Time after synchronization released (h)

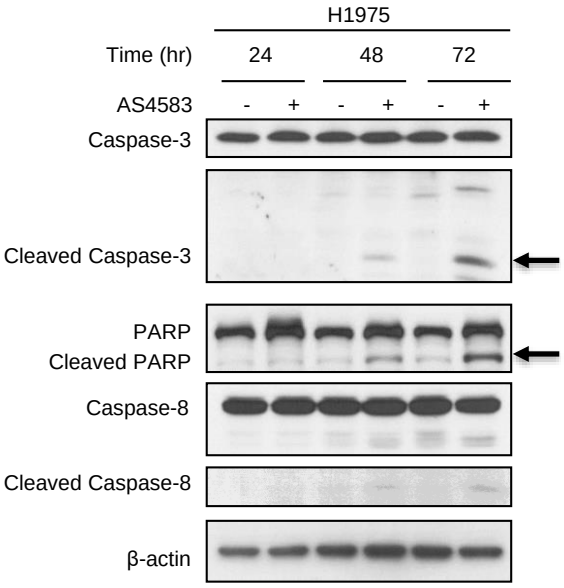
E
H1975
Time (hr)
24
48
72
AS4583
Caspase-3
Cleaved Caspase-3
PARP
Cleaved PARP
Caspase-8
Cleaved Caspase-8
β-actin

Lin et. al. Figure 3

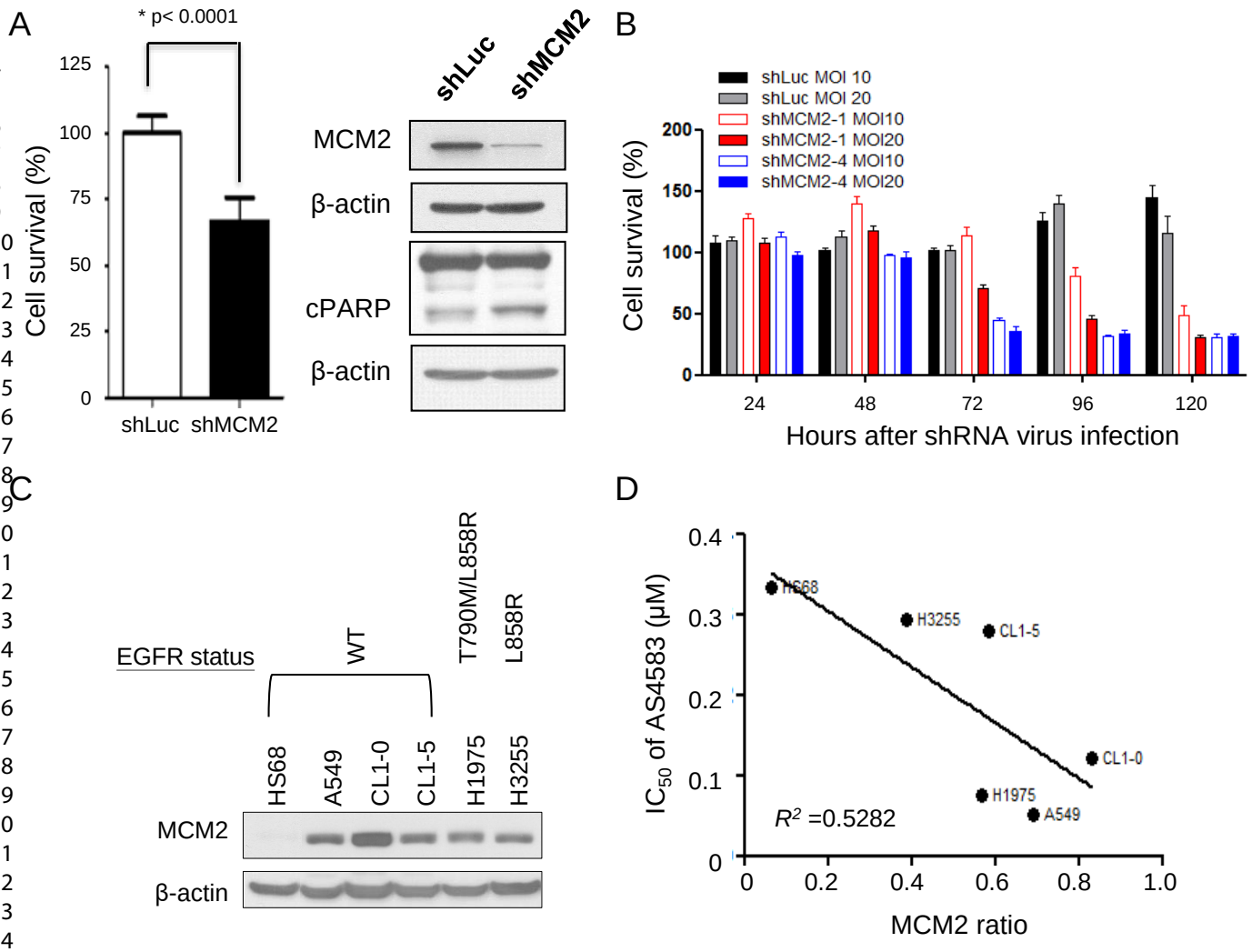

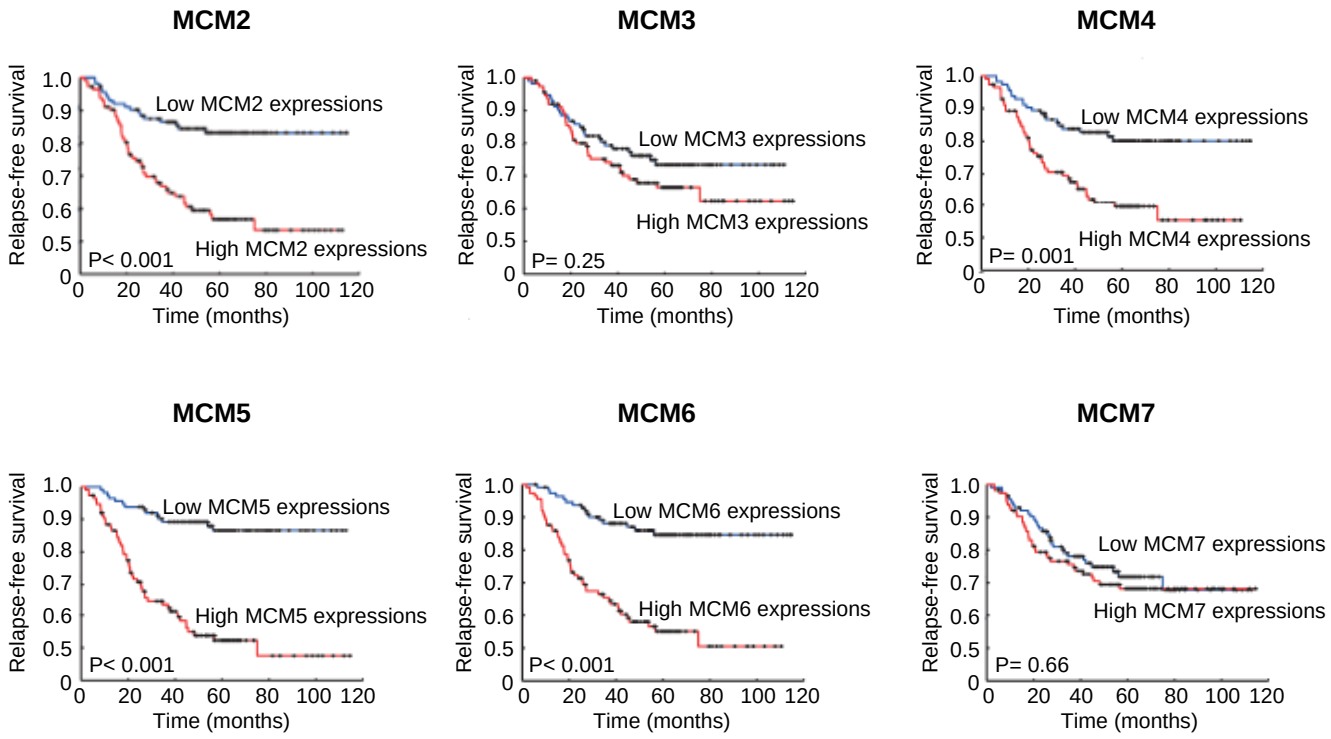
MCM2
Relapse-free survival
Low MCM2 expressions
High MCM2 expressions
P< 0.001
Time (months)
MCM3
Relapse-free survival
Low MCM3 expressions
High MCM3 expressions
P= 0.25
Time (months)
MCM4
Relapse-free survival
Low MCM4 expressions
High MCM4 expressions
P= 0.001
Time (months)
MCM5
Relapse-free survival
Low MCM5 expressions
High MCM5 expressions
P< 0.001
Time (months)
MCM6
Relapse-free survival
Low MCM6 expressions
High MCM6 expressions
P< 0.001
Time (months)
MCM7
Relapse-free survival
Low MCM7 expressions
High MCM7 expressions
P= 0.66
Time (months)

Lin et. al. Figure 5

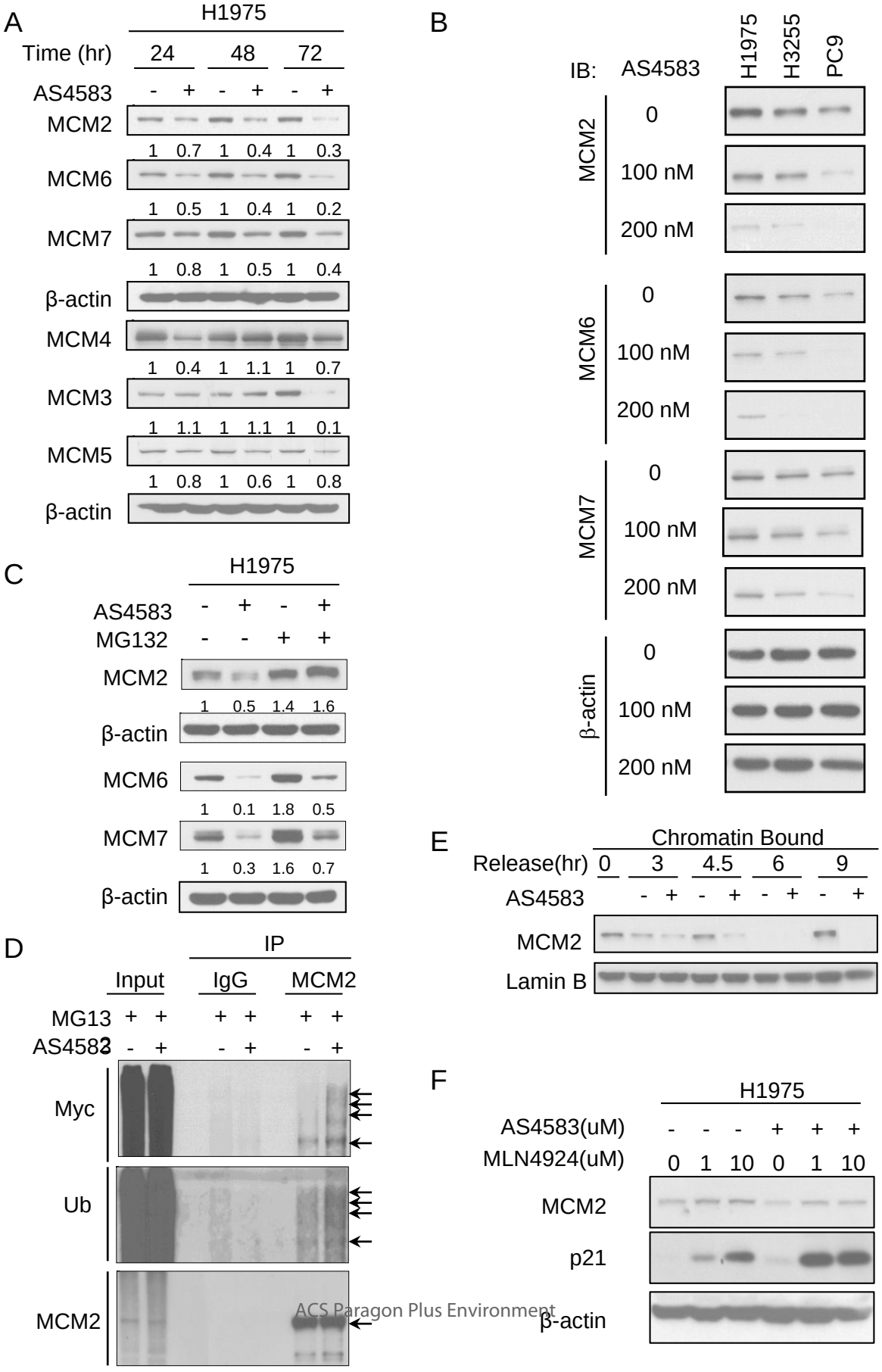

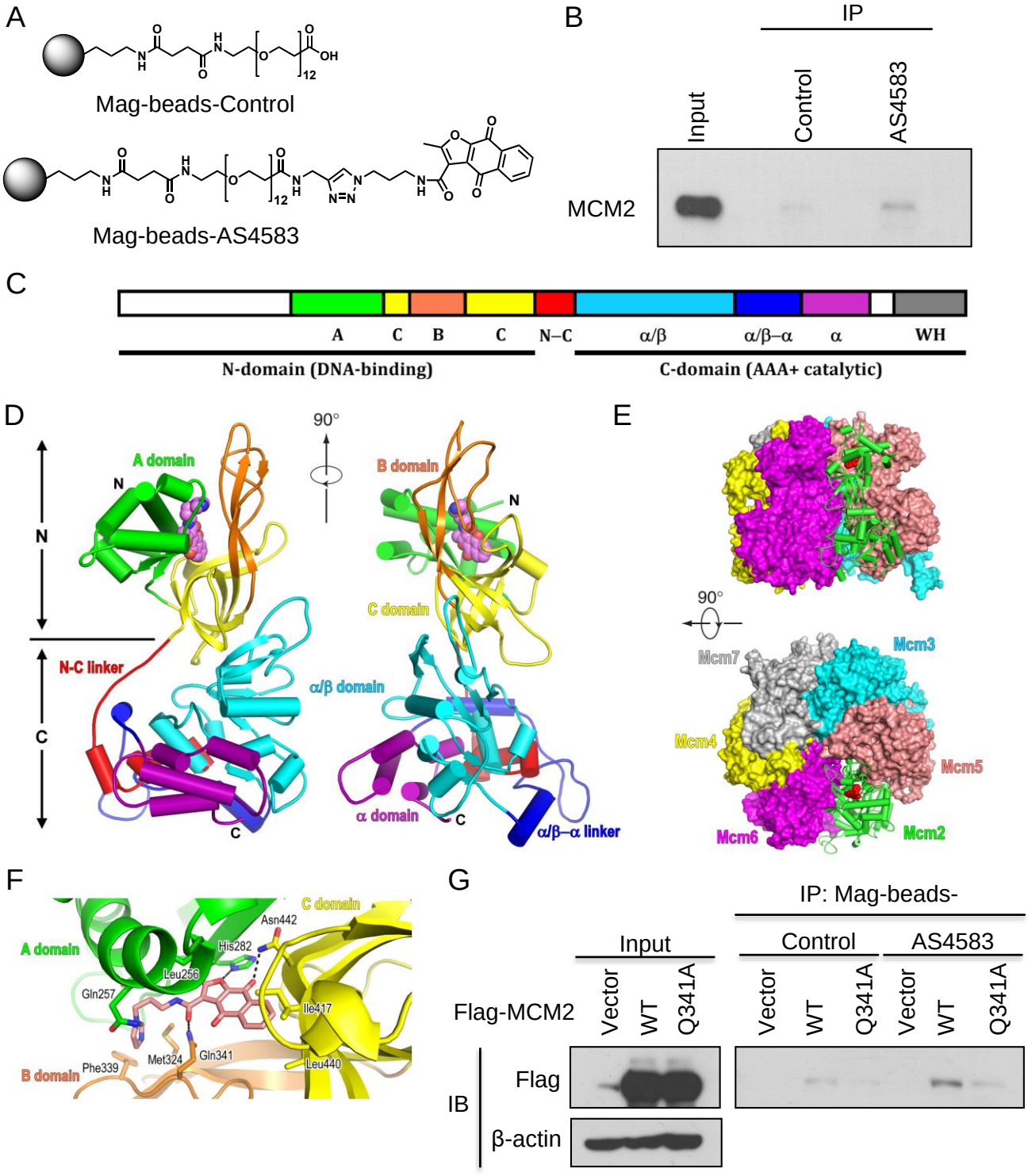
A
Mag-beads-Control
Mag-beads-AS4583
B
IP
Input
Control
AS4583
MCM2
C
A C B C N–C α/β α/β–α α WH
N-domain (DNA-binding)
C-domain (AAA+ catalytic)
D
90°
A domain
B domain
C domain
α/β domain
α domain
α/β–α linker
N-C linker
N
C
E
90°
Mcm3
Mcm7
Mcm4
Mcm5
Mcm6
Mcm2
F
A domain
B domain
C domain
Asn442
His282
Leu256
Gln257
Ile417
Met324
Gln341
Leu440
Phe339
G
IP: Mag-beads-
Input
Control
AS4583
Vector
WT
Q341A
Flag-MCM2
IB
Flag
β-actin

Lin et. al. Supplementary Figure 1

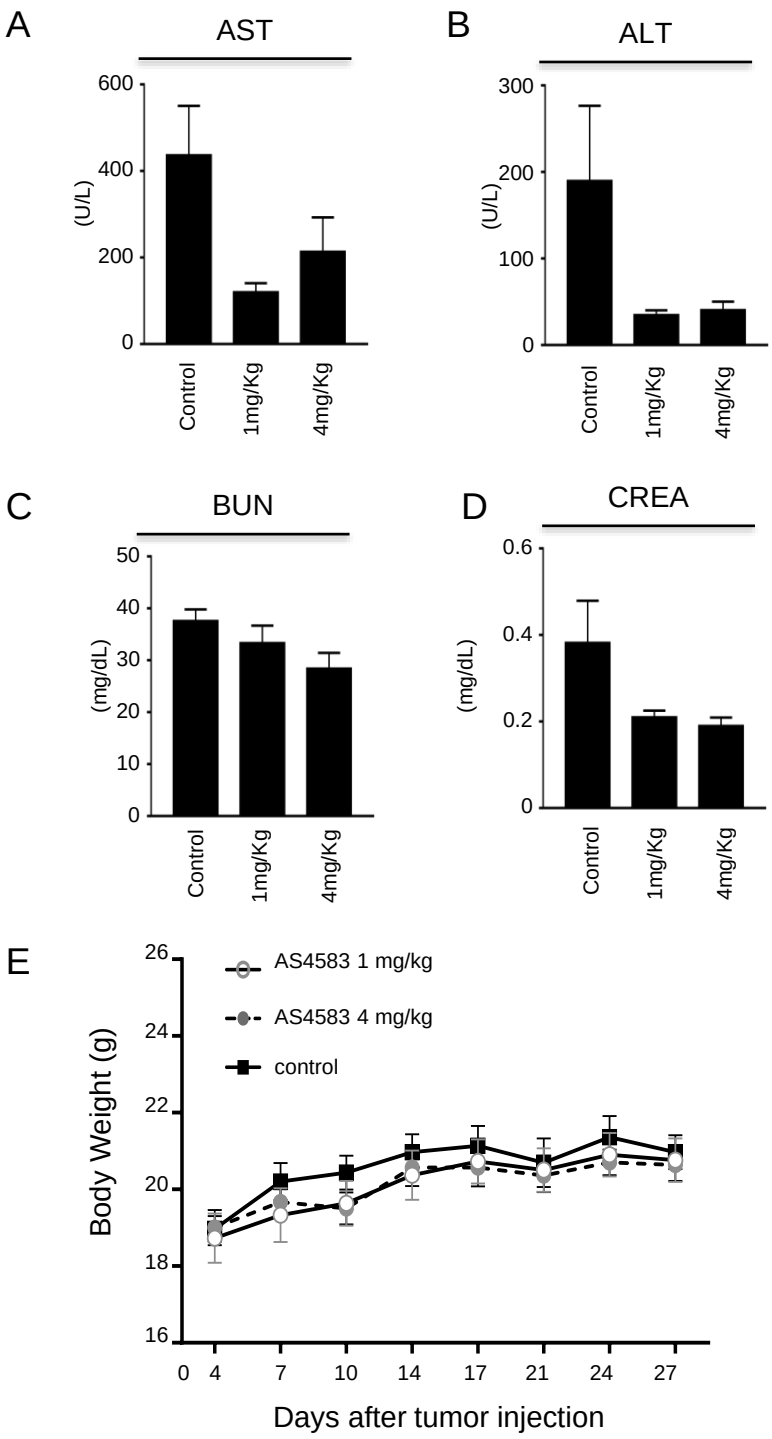

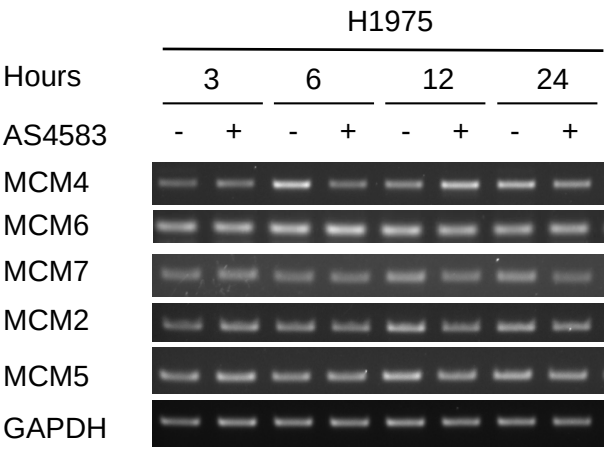
H1975
Hours
3
6
12
24
AS4583
- + - + - + - +
MCM4
MCM6
MCM7
MCM2
MCM5
GAPDH

Lin et. al. Supplementary Figure 3

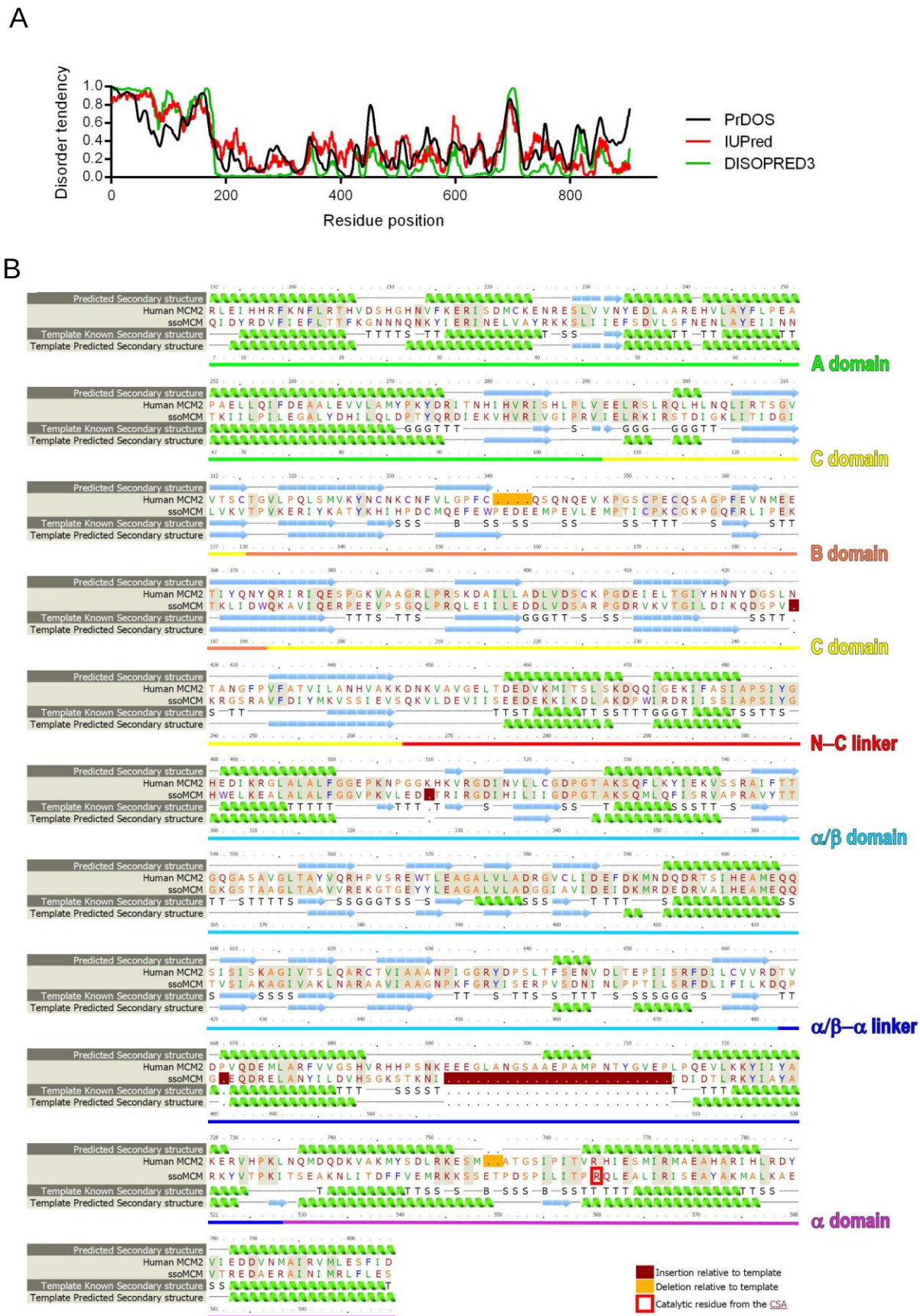

Lin et. al. Supplementary Figure 4

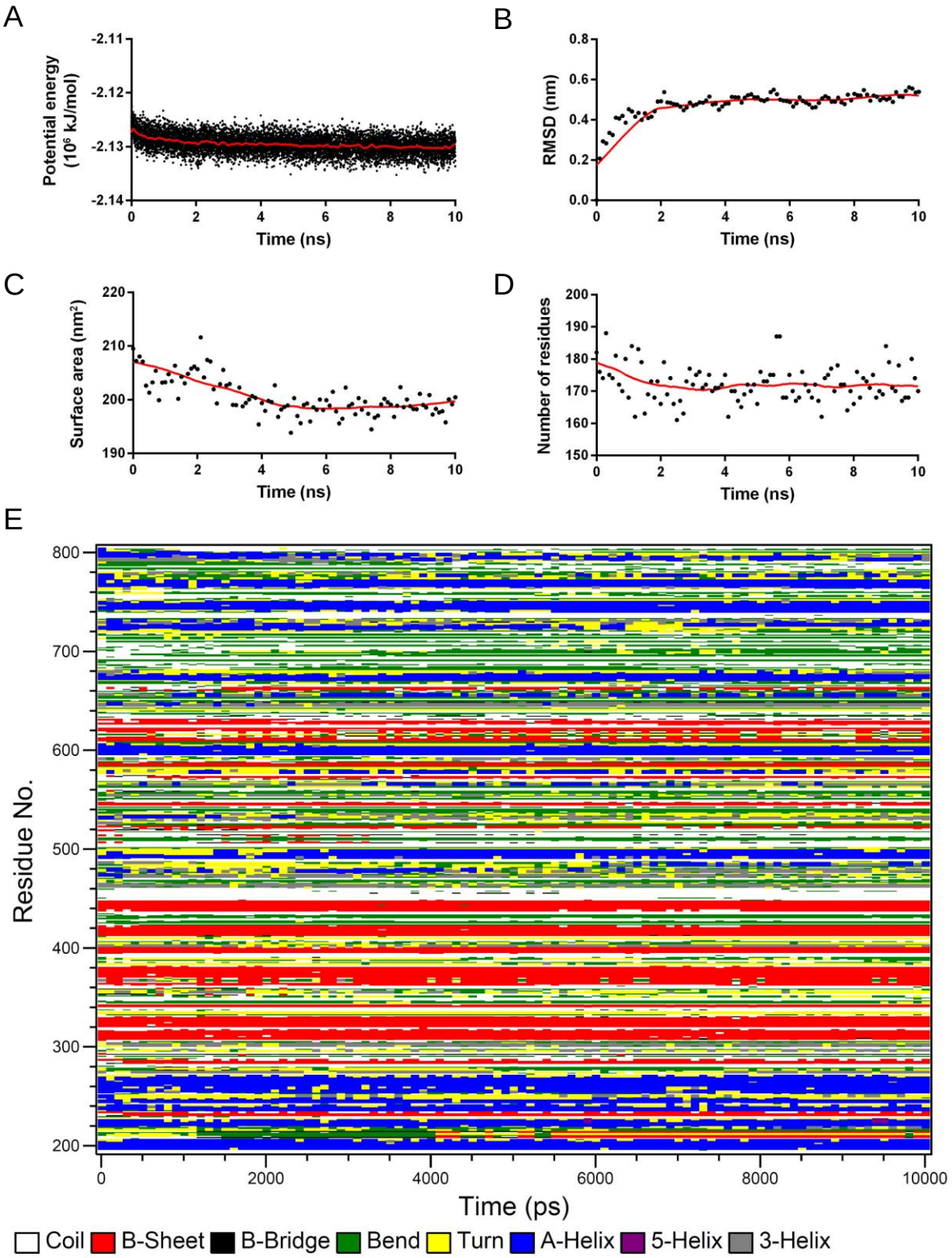

Lin et. al. Supplementary Figure 5

A

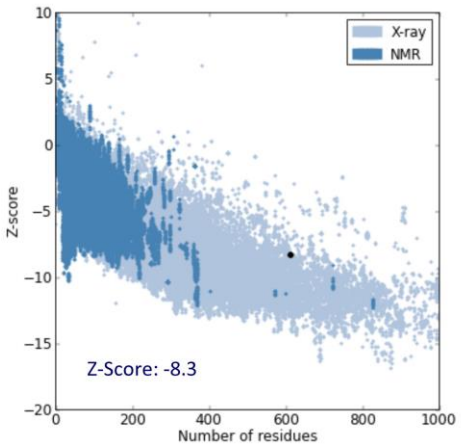

B

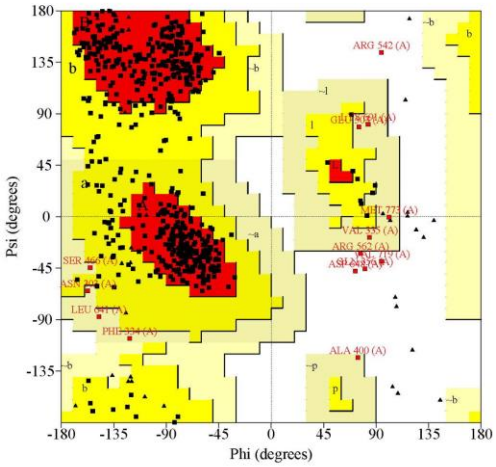

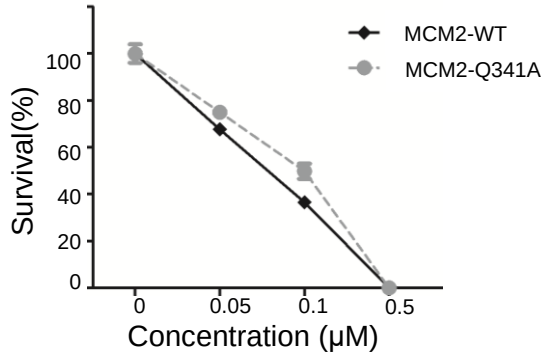
A
MCM2-WT
MCM2-Q341A
Survival(%)
100
80
60
40
20
0
0
0.05
0.1
0.5
Concentration (μM)

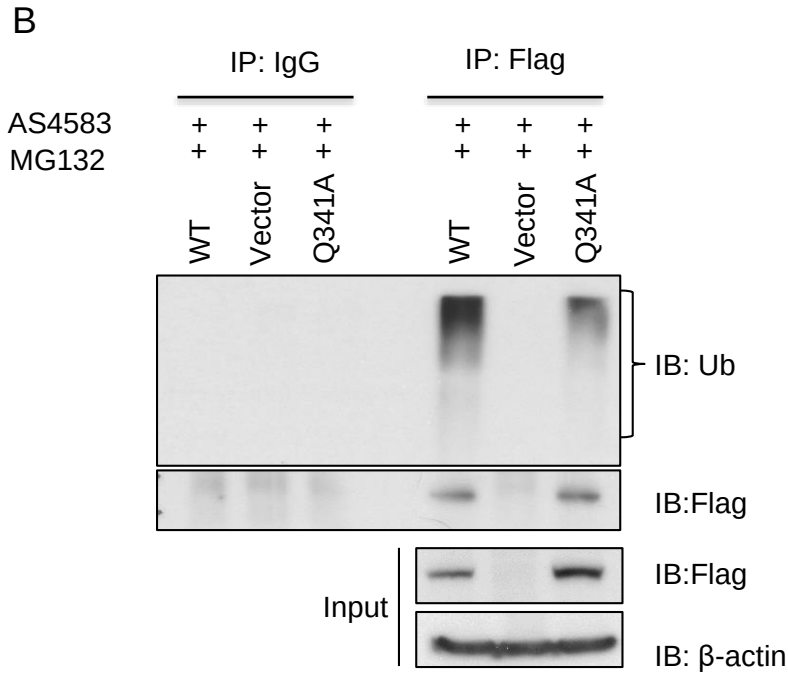
B
IP: IgG
IP: Flag
AS4583
MG132
WT
Vector
Q341A
IB: Ub
IB:Flag
Input
IB:Flag
IB: β-actin

Lin et al. Supplementary Figure 7